



Title	Intensive Hydration of the Wedge Mantle at the Kuril Arc-NE Japan Arc Junction : Implications from Mafic Lavas from Usu Volcano, Northern Japan
Author(s)	Kuritani, Takeshi; Tanaka, Mayumi; Yokoyama, Tetsuya; Nakagawa, Mitsuhiro; Matsumoto, Akiko
Citation	Journal of petrology, 57(6), 1223-1240 https://doi.org/10.1093/petrology/egw038
Issue Date	2016-06
Doc URL	http://hdl.handle.net/2115/65874
Rights	This is a pre-copyedited, author-produced PDF of an article accepted for publication in Journal of petrology following peer review. The version of record J Petrology 2016 57(6) 1223-1240 is available online at: https://doi.org/10.1093/petrology/egw038 .
Type	article (author version)
File Information	2016JPet.pdf



[Instructions for use](#)

1
2
3
4
5
6
7
8
9
10
11
12
13
14
15
16
17
18
19
20
21
22
23
24
25
26
27
28
29

Intensive hydration of the wedge mantle at the Kuril arc –
NE Japan arc junction:
Implications from mafic lavas from Usu Volcano,
northern Japan

Takeshi Kuritani^{1,2*}, Mayumi Tanaka^{1**}, Tetsuya Yokoyama³, Mitsuhiro
Nakagawa², Akiko Matsumoto²

¹Graduate School of Science, Osaka City University, Osaka, 558-8585, Japan

²Graduate School of Science, Hokkaido University, Sapporo, 060-0810, Japan

³Graduate School of Science and Engineering, Tokyo Institute of Technology, Tokyo,
152-8551, Japan

**Present address: Kyoto City Office, Kyoto, 604-8571, Japan

Email: kuritani@mail.sci.hokudai.ac.jp

Tel/Fax: +81-11-706-2729

30 **Abstract**

31 The generation and evolution of basaltic magmas at Usu volcano, located at the junction
32 between the NE Japan arc and the Kuril arc, have been investigated. The mafic products,
33 which form the somma edifice of the volcano, consist of basalt (49.6–51.3 wt % SiO₂)
34 and basaltic andesite (52.0–54.9 wt % SiO₂) lavas. The basaltic lavas show relatively
35 tight compositional trends, and ⁸⁷Sr/⁸⁶Sr ratios tend to decrease with increasing
36 whole-rock SiO₂ content. The water content of the basaltic magmas was determined to
37 be ~4.8 wt % based on plagioclase–melt thermodynamic equilibrium. Using this
38 information and an olivine maximum fractionation model, the water content of the
39 primary Usu magma was estimated to be 3.9 wt %. Multi-component thermodynamic
40 calculations suggest that the primary magma was generated by ~23% melting of the
41 source mantle with ~0.94 wt % H₂O at ~1300°C and ~1.4 GPa. The 0.94 wt % water
42 content of the source mantle is significantly higher than that beneath volcanoes in the
43 main NE Japan arc (generally <0.7 wt % H₂O); this implies that the wedge mantle at the
44 arc–arc junction is intensively hydrated. The temperature of the wedge mantle of
45 ~1300°C at ~1.4 GPa is also significantly higher than that of the mantle in the main NE
46 Japan arc. Unlike the basaltic lavas, the whole-rock compositions of the basaltic
47 andesite lavas are scattered in Harker variation diagrams. This observation suggests that
48 the compositional diversity was produced by at least two independent processes. To

49 elucidate the processes responsible for this compositional diversity, principal
50 component analysis was applied to the major element compositions of the samples. This
51 suggests that 47% of the diversity of the whole-rock compositions can be explained by
52 mixing with partial melts of lower crustal materials, 25% is explained by redistribution
53 of plagioclase phenocrysts, and 16% is explained by fractionation of accessory
54 minerals.

55

56 Key Words: arc–arc junction; magma generation; water content; wedge mantle;
57 magmatic differentiation

58

59 INTRODUCTION

60 Subduction-zone primary magmas are generated essentially by partial melting of the
61 wedge mantle through reactions with water-rich melts and fluids released from the
62 subducting plate (e.g. Ringwood, 1974; Sakuyama & Nesbitt, 1986; Tatsumi, 1986).
63 These processes are largely controlled by the thermal structure of the mantle, which is
64 in turn controlled by several factors such as the rate of convergence, temperature of the
65 downgoing plate, geometry of the subducting slab, and mantle wedge flow (Peacock,
66 2003). In some portions of some subduction zones, such as the main part of the NE
67 Japan arc, these factors are regarded to a first-order approximation as being essentially
68 constant in the along-arc direction. In this case, subduction-zone processes can be
69 examined by two-dimensional across-arc sections (e.g. Tatsumi, 1989; Iwamori, 1998;
70 Peacock & Wang, 1999; van Keken *et al.*, 2002), although some researchers have
71 suggested the need to consider along-strike second-order cyclic heterogeneity in the
72 thermal structure of the mantle (e.g. Tamura *et al.*, 2002; Honda *et al.*, 2007). However,
73 there are many other regions in which such a simple situation is not met. For example,
74 in the Central America arc, the subduction angle changes abruptly owing to slab rupture,
75 resulting in the segmentation of the volcanic front. In central Japan, where the
76 subducting Pacific and Philippine Sea plates overlap, magmatism is much more intense
77 than in the surrounding regions because of the enhanced fluid flux from the two

78 subducting plates (e.g. Nakamura *et al.*, 2008). In the Kamchatka arc, beneath which
79 oceanic islands (Hawaiian–Emperor seamount chain) are subducting, the magma
80 production rate is remarkably high at some volcanoes such as at Klyuchevskoy,
81 probably owing to the intensive fluid flux from the locally thickened oceanic crust of
82 the subducting Pacific slab (e.g. Dorendorf *et al.*, 2000).

83 The southwestern part of Hokkaido, northern Japan, is located at the junction
84 of the NE Japan arc and the Kuril arc (Fig. 1). The subducting Pacific plate beneath this
85 region shows a hinge-like shape owing to the dip change of the subducting plate along
86 the trench (Fig. 1). Because of the interest in this unique tectonic setting, this arc–arc
87 junction has been the focus of extensive geophysical studies (e.g. Wang & Zhao, 2005;
88 Miller *et al.*, 2006; Nakajima *et al.*, 2006; Kita *et al.*, 2010a; Morishige & van Keken,
89 2014). The surface morphology of the Pacific slab has been investigated in detail to
90 determine whether or not a slab tear is present in the distorted portion of the slab (e.g.
91 Katsumata *et al.* 2003; Miller *et al.*, 2006; Kennett & Furumura, 2010). Recent studies
92 with high-quality analysis have shown that the slab surface is continuous and that there
93 is no evidence of a slab tear (Miller *et al.*, 2006; Kennett & Furumura, 2010). The
94 three-dimensional velocity structure beneath Hokkaido has also been examined in detail
95 (e.g. Wang & Zhao, 2005, 2009; Nakajima *et al.*, 2006; Kita *et al.*, 2014), and
96 low-velocity and low-QP zones have been clearly imaged in the mantle wedge beneath

97 the active volcanoes.

98 Southwestern Hokkaido is also an area in which magmatism has been intense
99 (e.g. Tamura *et al.*, 2002). There are many active volcanoes such as Usu, Tarumae, and
100 Eniwa, and large calderas including Toya, Shikotsu, and Kuttara (Fig. 2). In this region,
101 the temporal and spatial evolution of volcanism and chemical compositions of the
102 volcanic rocks have been well characterized (e.g. Nakagawa, 1992). However, the
103 generation conditions of the parental magmas have not been estimated for these
104 volcanoes, probably because of the scarcity of basaltic products. Therefore, it remains
105 unclear whether the intensive magmatism of this region is linked to the unique tectonic
106 setting of the arc–arc junction.

107 In this study we carried out a petrological and geochemical investigation of
108 mafic lavas from Usu volcano (Fig. 1) and estimated the conditions under which the
109 magmas were generated. We selected this volcano because it is one of the few active
110 volcanoes in southwestern Hokkaido that has erupted basaltic products. The activity of
111 Usu volcano began with the formation of the present somma edifice (consisting of mafic
112 lavas) at ~30 ka (Miyabuchi *et al.*, 2014), followed by intermittent eruptions of felsic
113 magmas after AD 1663 (e.g. Soya *et al.*, 2007). Although the magmatic processes
114 responsible for the historic felsic products have been examined extensively (Oba, 1966,
115 1991; Katsui *et al.*, 1978; Okumura *et al.*, 1981; Oba *et al.*, 1983; Tomiya & Takahashi,

116 1995, 2005; Matsumoto *et al.*, 2005; Matsumoto & Nakagawa, 2010; Tomiya *et al.*,
117 2010), petrological and geochemical studies on the somma lavas are limited (e.g. Oba,
118 1964a, 1964b; Oba *et al.*, 1985; Fujimaki, 1986). These studies suggested that the
119 compositional variation of the somma lavas can be explained principally by fractional
120 crystallization. However, they were based on analytical data for only six samples, and
121 magmatic processes were not well constrained by high-quality geochemical data. In this
122 study we thoroughly examined the petrogenesis of the somma lavas using new
123 petrological and geochemical data and estimated the generation conditions of the
124 magmas. We also examined the compositional variation of the eruptive products to
125 understand the differentiation processes of the magmas.

126

127 **GEOLOGICAL SETTING AND SAMPLES**

128 Usu volcano, one of the most active volcanoes in Japan, consists of three lava domes
129 and more than 10 cryptodomes, along with a main stratovolcano (Fig. 2). After the
130 formation of Toya caldera (115–112 ka; Machida & Arai, 2003) and some post-caldera
131 volcanic activity, the main edifice of Usu volcano began to form on the southern rim of
132 the caldera with repeated eruptions of mafic lavas (somma lavas). According to Soya *et*
133 *al.* (2007) this magmatism occurred from 20 to 10 ka. However, Miyabuchi *et al.* (2014)
134 recently suggested that the volcano began its activity at ~30 ka on the basis of

135 tephrostratigraphy. After the formation of the main edifice, it collapsed to form the
136 Zenkoji debris avalanche deposit (Fig. 2). There was a long dormancy after the mafic
137 magmatism, but volcanic activity resumed in AD 1663 with the eruption of rhyolitic
138 magma. Since then, the volcano has erupted eight times, in AD<1769, 1769, 1822, 1853,
139 1910, 1943–1945, 1977–1978, and 2000 (Yokoyama *et al.*, 1973; Soya *et al.*, 1981;
140 Nakagawa *et al.*, 2005). The volcanic products erupted in historical times are felsic;
141 their SiO₂ contents tend to decrease systematically with time from 74–76wt % (AD
142 1663) to ~69 wt % (AD 2000) (Oba, 1966; Nakagawa *et al.*, 2002, 2005; Matsumoto &
143 Nakagawa, 2010).

144 The somma lavas, which were investigated in this study, have basaltic and
145 basaltic andesitic compositions (Oba, 1964b). The lavas are exposed extensively on the
146 flanks of the somma edifice (Fig. 2). The volume of the somma lavas, including those
147 emplaced as the Zenkoji debris avalanche deposit, is estimated to be ~0.5 km³
148 (Miyabuchi *et al.*, 2014). Oba (1964a) divided the somma lavas into seven types on the
149 basis of the distribution and petrographic features of the products. In this study, 82
150 samples were collected from the somma lavas (Fig. 2). In addition, one sample of
151 plutonic rock, which may be representative of the upper crust beneath Usu volcano, was
152 collected from Kimobetsu (Fig. 2). Whole-rock analysis using X-ray fluorescence
153 (XRF) spectrometry was performed for all of these samples. Trace element

154 concentrations and Sr, Nd, and Pb isotopic compositions were determined for 38
155 selected samples of the somma lavas, as well as the plutonic rock sample from
156 Kimobetsu. In addition, Sr isotopic analyses were carried out for 12 separates of
157 plagioclase phenocrysts from three somma lava samples, and Sr, Nd, and Pb isotopic
158 compositions were determined for two samples of lower crustal xenoliths (hornblende
159 gabbro) from Ichinome-gata (Megata volcano in Fig. 1; e.g. Aoki, 1971).

160

161 **ANALYTICAL METHODS**

162 For whole-rock analysis, rock specimens were crushed to coarse chips of 3–5 mm
163 diameter, from which fresh chips were hand-picked. The chips were rinsed with
164 deionized water in an ultrasonic bath for at least 3 h and were then dried at 110°C for
165 >12 h. The washed chips were ground using an alumina mill. Powdered samples were
166 kept at 950°C for more than 12 h in a muffle furnace, and loss on ignition (LOI) was
167 obtained gravimetrically.

168

169 **Whole-rock major and trace elements**

170 Concentrations of whole-rock major and some trace elements (V, Co, and Ni) were
171 determined by XRF using a Rigaku RIX 2100 at the Graduate School of Science, Osaka
172 City University. Glass beads were prepared by fusion with an alkali flux (2:1 sample

173 dilution) consisting of a 4:1 mixture of lithium tetraborate and lithium metaborate. The
174 analytical techniques have been described by Suda *et al.* (2010). The composition of the
175 GSJ reference material JB-3 (basalt from Mt Fuji) measured in the course of this study,
176 along with its reference value (Imai *et al.*, 1995), are listed in table 1 of Kuritani *et al.*
177 (2013). Additional trace elements were analyzed by inductively coupled plasma mass
178 spectrometry (ICP-MS) using a Thermo Fisher Scientific X-series II at the Graduate
179 School of Science and Technology, Tokyo Institute of Technology, following the
180 methods of Yokoyama *et al.* (in preparation) for Rb, Sr, Y, Cs, Ba, rare earth elements
181 (REE), Pb, Th, and U, and Lu *et al.* (2007) for Zr, Nb, Hf, and Ta. In the method of
182 Yokoyama *et al.* (in preparation), an ^{113}In – ^{203}Tl double spike is added to the powdered
183 samples and the sample–spike mixtures are decomposed by acids using the method of
184 Yokoyama *et al.* (1999). Final solutions are prepared in 0.5N HNO_3 with a dilution
185 factor of ~5000, and the elemental concentrations are determined by isotope
186 dilution–internal standardization. All of the analyses were duplicated for each sample,
187 and always showed a relative per cent difference of less than 3–5%.

188

189 **Sr–Nd–Pb isotopes**

190 The analytical procedures for chemical separation followed the methods of Pin *et al.*
191 (1994) and Noguchi *et al.* (2011) for Sr, Pin *et al.* (1994) and Pin & Zalduegui (1997)

192 for Nd, and Kuritani & Nakamura (2002) for Pb. Isotopic ratios were determined with a
193 multiple collector (MC)-ICP-MS system (Neptune plus, Thermo Fisher Scientific) at the
194 Graduate School of Science, Hokkaido University. Mass fractionation factors for Sr and
195 Nd were internally corrected using $^{86}\text{Sr}/^{88}\text{Sr} = 0.1194$ and $^{146}\text{Nd}/^{144}\text{Nd} = 0.7219$,
196 respectively, and those for Pb were corrected using Tl as an external standard.
197 Additional corrections were performed by applying a standard bracketing method using
198 NIST987, JNdi-1, and NIST981 for Sr, Nd, and Pb isotopic analyses, respectively, and
199 the data were finally normalized to $^{87}\text{Sr}/^{86}\text{Sr} = 0.710214$ for NIST 987, $^{143}\text{Nd}/^{144}\text{Nd} =$
200 0.512117 for JNdi-1, and $^{206}\text{Pb}/^{204}\text{Pb} = 16.9424$, $^{207}\text{Pb}/^{204}\text{Pb} = 15.5003$, and $^{208}\text{Pb}/^{204}\text{Pb}$
201 $= 36.7266$ for NIST981 (Kuritani & Nakamura, 2003). The isotopic ratios of the GSJ
202 standard JB-3, measured in the course of this study, were $^{87}\text{Sr}/^{86}\text{Sr} = 0.703375 \pm 20$ ($n =$
203 7 , 2SD), $^{143}\text{Nd}/^{144}\text{Nd} = 0.513065 \pm 2$ ($n = 3$, 2SD), and $^{206}\text{Pb}/^{204}\text{Pb} = 18.2962 \pm 10$,
204 $^{207}\text{Pb}/^{204}\text{Pb} = 15.5393 \pm 14$, and $^{208}\text{Pb}/^{204}\text{Pb} = 38.2545 \pm 27$ ($n = 5$, 2SD).

205

206 **Mineral chemistry**

207 The mineral compositions of the lavas were determined using a JEOL JXA-8800
208 electron microprobe at the Graduate School of Science, Hokkaido University. The
209 operating conditions for mafic minerals were as follows: accelerating voltage, 15 kV;
210 beam current, 12 nA; counting time, 20 s. To analyze the composition of plagioclase, an

211 accelerating voltage of 15 kV and a beam current of 10 nA were used; the counting time
212 was 10 s and the beam diameter was 10 mm. Both oxide and natural mineral standards
213 were used, and data were obtained using the ZAF correction method.

214

215 **PETROGRAPHY AND MINERAL CHEMISTRY**

216 Photomicrographs of representative samples are shown in Fig. 3, and the modal
217 compositions of phenocrysts (defined as having diameter or length >0.3 mm for
218 plagioclase and >0.1 mm for mafic minerals) of selected samples are listed in Table 1.

219 The somma lavas are porphyritic, and generally contain orthopyroxene, clinopyroxene
220 and plagioclase phenocrysts. Plagioclase megacrysts (>1 cm in length) are rarely
221 present. As described below, on the basis of whole-rock compositions, the somma lavas
222 can be divided into basalt and basaltic andesite samples, and the latter group is further
223 divided into low- and high-P₂O₅ samples. Olivine phenocrysts are found in basalt
224 samples and some basaltic andesite samples. In the basalt samples, the modal
225 compositions of olivine phenocrysts decrease systematically with increasing whole-rock
226 SiO₂ content (Table 1). The olivine phenocrysts are commonly rounded (Fig. 3a) and
227 some have a reaction rim of orthopyroxene. Pyroxene phenocrysts are typically less
228 than 2mm in length, but phenocrysts up to 5mm are occasionally present. Some
229 pyroxene phenocrysts are rounded. Plagioclase phenocrysts, usually less than 3 mm in

230 length, have euhedral outlines.

231 The olivine phenocrysts are normally zoned in terms of Mg# [$100 \times \text{Mg}/(\text{Mg} +$
232 $\text{Fe}^{2+})$]. The Mg#s of the cores of the olivine phenocrysts show a bimodal distribution in
233 each basaltic sample (Fig. 4). The higher-Mg# (76–80) phenocrysts and the lower-Mg#
234 (60–75) phenocrysts are commonly larger and smaller than ~0.5 mm, respectively. The
235 Mg#s of the higher-Mg# olivine phenocrysts are essentially similar throughout the
236 basalt lavas, whereas those of the lower-Mg# phenocrysts decrease from 66–75 (e.g.
237 Usu#10; Fig. 4) to 60–70 (e.g. Usu#47b) with increasing whole-rock SiO₂ content of the
238 host sample. The orthopyroxene and clinopyroxene phenocrysts in basalt samples have
239 Mg# of 69–76, and those in basaltic andesite samples have Mg# of 66–74. The
240 plagioclase phenocrysts in basalt samples are generally homogeneous with respect to
241 An content [$100 \times \text{Ca}/(\text{Ca} + \text{Na})$], except for the rims. The An contents of the
242 phenocryst cores are mostly in the range 85–94 (Fig. 5a), and concentrated within the
243 range of 92–93, irrespective of the whole-rock SiO₂ content of the samples. In basaltic
244 andesite samples, the An contents of the cores of plagioclase phenocrysts show a
245 bimodal distribution. The An contents of one mode range from ~85 to ~94 and those of
246 the other mode range from ~75 to ~85 (Fig. 5b and c). The high-An core (>An85) in
247 some phenocrysts is surrounded by a mantle with relatively low An content (An75–85)
248 with a range similar to that of the low-An mode.

249 Figure 6 shows the relationship between the Mg# of pyroxene phenocrysts and
250 the An content of plagioclase crystals, which show evidence of simultaneous growth in
251 the same crystal aggregates. The Mg# of the pyroxene phenocrysts is positively
252 correlated with the An content of plagioclase. In basaltic samples, the high-An
253 plagioclase phenocrysts (>An85) coexist with pyroxene phenocrysts with \sim Mg#72. It
254 is noteworthy that plagioclase phenocrysts with >An91 do not form crystal aggregates
255 with pyroxene phenocrysts. The large olivine phenocrysts with higher Mg# (76–80)
256 commonly occur as isolated grains.

257

258 **WHOLE-ROCK COMPOSITION**

259 Whole-rock major and trace element and Sr, Nd, and Pb isotopic compositions of
260 representative samples of the somma lavas, as well as the plutonic rock sample from
261 Kimobetsu (Mrtk#1), are reported in Table 2 and in Table A1 (Supplementary Data,
262 available for downloading at <http://petrology.oxfordjournals.org>). Figure 7 shows
263 Harker variation diagrams for some major oxides (TiO₂, Al₂O₃, MgO, CaO, K₂O, and
264 P₂O₅) plotted against SiO₂. The SiO₂ content of the somma lavas ranges from 49.6 to
265 54.9 wt %, and they can be clearly divided into basalt (<51.4 wt % SiO₂) and basaltic
266 andesite (>52.0 wt % SiO₂) samples. The basalt lavas belong to Stage 1 of Oba (1964a)
267 and are considered to have erupted in the earliest stage of the somma activity. Although

268 the basalt samples form relatively tight compositional trends in Harker diagrams, the
269 data for the basaltic andesite samples are scattered in compositional space. In particular,
270 the basaltic andesite lavas show large variations in P_2O_5 content; for example, from
271 ~ 0.08 to ~ 0.2 wt % at the SiO_2 content of 53 wt %. On the basis of this observation, the
272 basaltic andesite samples have been subdivided into low- P_2O_5 ($< \sim 0.12$ wt %) and
273 high- P_2O_5 ($> \sim 0.12$ wt %) sub-groups (Fig. 7). In some localities, lava flows of the
274 high- P_2O_5 basaltic andesite are underlain by a layer of scoria with a low- P_2O_5
275 composition (Miyabuchi *et al.*, 2014). This observation suggests that eruptions of the
276 low- P_2O_5 products predated those of the high- P_2O_5 products. It is thus suggested that
277 the activity of the somma magmas began with the eruption of the basalt lavas, followed
278 by the eruption of the low- P_2O_5 basaltic andesite products, and ended with the eruption
279 of the high- P_2O_5 basaltic andesite products. The plutonic rock sample from Kimobetsu
280 (Mrtk#1) has a SiO_2 content of ~ 60 wt % and is thus classified as diorite.

281 Figure 8 shows variation diagrams for Ni, Sr, and Y plotted against SiO_2
282 content. The Sr and Y concentrations of the high- P_2O_5 basaltic andesite samples tend to
283 be higher than those of the low- P_2O_5 basaltic andesite samples at a given SiO_2 content.
284 A primitive mantle (PM)-normalized multi-element concentration diagram is shown in
285 Fig. 8d. The pattern is characterized by negative anomalies of Nb and Ta and positive
286 spikes in Pb and Sr. These features are characteristic of subduction-related magmas.

287 Variations of Sr, Nd, and Pb isotopic composition with SiO₂ content are shown
288 in Fig. 9a–c. Interestingly, in the basalt samples, ⁸⁷Sr/⁸⁶Sr and ²⁰⁶Pb/²⁰⁴Pb tend to
289 decrease with increasing SiO₂ content. The ⁸⁷Sr/⁸⁶Sr and ¹⁴³Nd/¹⁴⁴Nd compositions of
290 the basalt samples are similar to those of the basaltic andesite samples (Fig. 9a and b).
291 In contrast, the basaltic andesite samples have lower ²⁰⁶Pb/²⁰⁴Pb than the basalt samples
292 (Fig. 9c), and ²⁰⁶Pb/²⁰⁴Pb tends to decrease systematically with increasing P₂O₅ content
293 (Fig. 9d). The diorite sample has ⁸⁷Sr/⁸⁶Sr of ~0.7049 and ¹⁴³Nd/¹⁴⁴Nd of ~0.5127,
294 which are significantly higher and lower, respectively, than those of the somma lava
295 samples (Fig. 10a). The Sr, Nd, and Pb isotopic ratios of the lower crustal samples are
296 listed in Table 3 (Nd isotopic analysis was carried out for only one sample). They have
297 relatively low ²⁰⁶Pb/²⁰⁴Pb and high ⁸⁷Sr/⁸⁶Sr compared with those of the somma lavas
298 (Fig. 10). The ⁸⁷Sr/⁸⁶Sr composition of the separates of the high-An plagioclase
299 phenocrysts from two basalt samples (Usu#10 and Usu#64) and one basaltic andesite
300 sample (Usu#16) are listed in Table 4. The ⁸⁷Sr/⁸⁶Sr ratios of the plagioclase
301 phenocrysts are mostly constant at ~0.70380, irrespective of the whole-rock
302 composition of the host-rocks, and are similar to the lowest ratios in the somma lava
303 samples.

304

305 **GENERATION CONDITIONS OF THE MAGMAS**

306 **Origin of the compositional diversity of the basalt lavas**

307 The basaltic lavas show relatively tight whole-rock compositional trends and the
308 $^{87}\text{Sr}/^{86}\text{Sr}$, $^{206}\text{Pb}/^{204}\text{Pb}$, and $^{208}\text{Pb}/^{204}\text{Pb}$ ratios change systematically with the whole-rock
309 SiO_2 content (Figs 7–9). Therefore, it can be considered that the compositional diversity
310 of the lavas was produced by either (1) combined assimilation and fractional
311 crystallization (AFC) or (2) mixing of magmas with distinct isotopic compositions. Of
312 these two hypotheses, the former is not likely to be true. If AFC was the cause, the
313 lowest SiO_2 samples (such as Usu#10) should be close to the parental magma. In this
314 parental magma, olivine, plagioclase, and possibly orthopyroxene would have been the
315 main crystallizing phases, as inferred from the phenocryst assemblage of the lowest
316 SiO_2 basalt samples (Table 1). However, the $^{87}\text{Sr}/^{86}\text{Sr}$ ratios of the plagioclase
317 phenocrysts are significantly different from those of the lowest SiO_2 samples (i.e.
318 Usu#10) and are rather similar to those of the most-evolved (i.e. highest SiO_2) basaltic
319 samples (i.e. Usu#64). This observation is not consistent with AFC processes.

320 From these observations, it is suggested that the compositional diversity of the
321 basalt lavas was produced primarily by magma mixing. In this case, the composition of
322 the higher SiO_2 end-member magma is considered to be close to that of Usu#64,
323 because the $^{87}\text{Sr}/^{86}\text{Sr}$ ratios of the plagioclase phenocrysts are similar to those of the
324 higher SiO_2 basalt lavas (Fig. 9a). On the other hand, a lower SiO_2 end-member magma

325 may have a composition with ~ 49.7 wt % SiO_2 based on extrapolation of the
326 whole-rock compositional trends of the basalt lavas. It is plausible that the higher-Mg#
327 olivine phenocrysts were derived from the lower- SiO_2 endmember magma, whereas the
328 high-An plagioclase phenocrysts, as well as orthopyroxene and clinopyroxene
329 phenocrysts, were derived from the higher- SiO_2 end-member magma, because the
330 pyroxene phenocrysts show evidence of contemporaneous growth with the high-An
331 plagioclase phenocrysts. Although the modal abundance of the olivine phenocrysts
332 decreases with increasing whole-rock SiO_2 content, those of the plagioclase and
333 pyroxene phenocrysts do not show systematic variations with SiO_2 content (Table 1).
334 This observation suggests that redistribution of these phenocryst phases might have
335 occurred in the magmas after magma mixing. In the basalt lavas both lower-Mg#
336 olivine phenocrysts and higher-Mg# olivine phenocrysts are present (e.g. Fig. 4).
337 Because the Mg#s of the lower-Mg# olivine phenocrysts decrease with increasing
338 whole-rock SiO_2 content, these phenocrysts are considered to have formed after the
339 compositional trend of the basalt magmas was established by magma mixing.

340

341 **Water content condition of the basaltic somma magmas**

342 As discussed above, the SiO_2 -rich basaltic lavas (e.g. Usu#64) represent an end-member
343 magma and did not experience a significant magma mixing event, as suggested from the

344 isotopic equilibrium of the plagioclase phenocrysts with the host sample. In addition,
345 for Usu#64, the europium anomaly, which is defined as $[Eu]_N = 2/([Sm]_N + [Gd]_N)$,
346 where the subscript N denotes the primitive mantle-normalized ratio, is close to unity,
347 suggesting that the plagioclase phenocrysts with An contents up to 94 were grown in
348 situ in the Usu#64 magma. On the basis of these observations, the water content was
349 estimated for the Usu#64 magma based on plagioclase–melt thermodynamic
350 equilibrium, given that the cores of the plagioclase phenocrysts with the highest An
351 content of 94 are in thermodynamic equilibrium with a melt with the composition of
352 Usu#64.

353 In this study, the plagioclase–melt hygrometer of Putirka (2008) was used. To
354 reliably estimate a water content using this hygrometer, the pressure and temperature
355 conditions need to be known. The pressure condition was estimated for the Usu#64
356 magma using the compositions of the clinopyroxene phenocrysts and the coexisting
357 orthopyroxene phenocrysts; these phases show evidence of simultaneous growth with
358 the An-rich plagioclase phenocrysts with up to An91 (Fig. 6). By applying the
359 two-pyroxene geothermobarometer of Putirka (2008) to 14 cpx–opx pairs, a
360 crystallization pressure of 0.65 ± 0.6 GPa and a crystallization temperature of $1018 \pm$
361 14°C was obtained. However, this represents the temperature at which plagioclase
362 phenocrysts with up to An91 were grown; plagioclase phenocrysts of composition An94

363 are considered to have been crystallized at higher temperatures than 1018°C. The
364 crystallization temperature of the plagioclase with An₉₄ was constrained using equation
365 26 of Putirka (2008), which calculates the liquidus temperature of plagioclase for a melt.
366 By simultaneously solving equation (25b) and equation (26) of Putirka (2008) at the
367 pressure condition of 0.65 GPa, a water content of 4.8 wt% and a temperature of
368 ~1090°C were obtained. The uncertainty of the estimated water content using this
369 hygrometer is 1.1 wt% (Putirka, 2008).

370

371 **Primary magma composition for the somma basalt lavas**

372 A water content of 4.8 ± 1.1 wt % was obtained for the Usu#64 magma, as described
373 above. However, this magma has an MgO content of 6.1 wt %, which is too low to be in
374 equilibrium with the upper mantle. This observation suggests that the Usu#64 magma
375 was significantly differentiated from a primary magma generated in the upper mantle.
376 The alphaMELTS model in the MELTS mode (Ghiorso & Sack, 1995; Asimow &
377 Ghiorso, 1998; Smith & Asimow, 2005) suggests that olivine should be the sole
378 liquidus phase in the Usu#64 magma at 0.65 GPa. As described above, the europium
379 anomaly of the Usu#64 magma is close to unity, suggesting that the primary magma
380 evolved to the Usu#64 magma without significant fractionation of plagioclase. In
381 addition, the An contents of plagioclase phenocrysts that form crystal aggregates with

382 pyroxene phenocrysts are lower than 91 (Fig. 6), suggesting that orthopyroxene and
383 clinopyroxene appeared as crystallization phases in the Usu#64 magma after the
384 significant crystallization of plagioclase. This is supported by the lower crystallization
385 temperatures of pyroxenes of ~1020°C compared with ~1090°C at which the liquidus
386 An₉₄ plagioclase began to form. From these results, it is plausible that the Usu#64
387 magma differentiated from a primary magma solely by fractional crystallization of
388 olivine and that the magma was then cooled to form plagioclase phenocrysts at 0.65
389 GPa, followed by crystallization of clinopyroxene and orthopyroxene phenocrysts. In
390 this case, the primary magma composition for Usu#64 can be estimated by the olivine
391 maximum fractionation model; that is, incremental addition of equilibrium olivine to the
392 melt until the melt could coexist with mantle olivine (Tatsumi *et al.*, 1983).

393 At each incremental step (0.5 wt % olivine), the Mg# of the equilibrium olivine
394 and the ferric–ferrous ratio of the melt were calculated using the alphaMELTS model at
395 an oxygen fugacity of NNO₁, where NNO is the nickel–nickel oxide buffer (e.g.
396 Righter *et al.*, 2008). The calculation showed that an addition of 19 wt % equilibrium
397 olivine to the Usu#64 sample is required for the magma to equilibrate with mantle
398 olivine with Mg#91.5 (note that the Mg#91.5 of the mantle olivine was determined
399 through iterative calculations so that this Mg# is consistent with the prediction by the
400 alphaMELTS model at a given degree of melting of the source mantle estimated below).

401 In this case, the SiO₂ and MgO contents of the primary magma are 49.2 wt % and 14.0
402 wt %, respectively (Table 2). The water content is estimated to be 3.9 ± 0.9 wt %, given
403 that the uncertainty results solely from that of the estimation using the plagioclase–melt
404 hygrometer of Putirka (2008).

405

406 **Flux melting of the source mantle**

407 There is a consensus that the source mantle for arc magmas is depleted mid-ocean ridge
408 basalt (MORB)-source mantle (DMM) and that primary arc magmas are generated
409 through melting of DMM by the influx of slab-derived water-rich melts or fluids
410 derived from an altered oceanic crust (AOC) component and a sediment (SED)
411 component (White & Dupré, 1986; Ellam & Hawkesworth, 1988; Ishikawa &
412 Nakamura 1994; Elliott, 2003, and references therein). The Pb isotopic compositions of
413 the basaltic somma lavas lie within the triangular field defined by DMM, AOC (Pacific
414 MORB), and SED (Pacific sediments) components (Fig. 10b), suggesting that the Pb
415 isotopic composition of magmas can indeed be represented by mixtures of these three
416 components.

417 The relative contributions of the DMM, AOC and SED components to the
418 source of the primary Usu magma were estimated using the Pb isotopic compositions
419 and the Pb concentrations of the three components. The primary magma can be

420 considered to be a mixture of the DMM component and a slab-derived fluid consisting
421 of the AOC and SED components. Therefore, the Pb isotopic composition of the
422 slab-derived fluid is the intersection point between the line passing through the
423 compositions of the DMM component and the basalt lavas and the line passing through
424 the compositions of the AOC and SED components in a $^{208}\text{Pb}/^{204}\text{Pb}$ – $^{206}\text{Pb}/^{204}\text{Pb}$ diagram
425 (Fig. 10b). By this process, a composition of $^{206}\text{Pb}/^{204}\text{Pb} = 18.67$, $^{207}\text{Pb}/^{204}\text{Pb} = 15.65$,
426 and $^{208}\text{Pb}/^{204}\text{Pb} = 38.65$ was obtained (open square in Fig. 10b). The Pb isotopic
427 composition of the AOC component is assumed to be $^{206}\text{Pb}/^{204}\text{Pb} = 18.54$, $^{207}\text{Pb}/^{204}\text{Pb} =$
428 15.45 , $^{208}\text{Pb}/^{204}\text{Pb} = 37.7$, with Pb = 0.44 ppm, and that of the SED component is
429 assumed to be $^{206}\text{Pb}/^{204}\text{Pb} = 18.70$, $^{207}\text{Pb}/^{204}\text{Pb} = 15.70$, and $^{208}\text{Pb}/^{204}\text{Pb} = 38.9$, with Pb
430 = 15.4 ppm (Kimura & Nakajima, 2014; Fig. 10b). Thus, the Pb isotopic ratios of the
431 slab-derived fluid can be explained by a 9:1 mixture of the AOC component and the
432 SED component.

433 The primary Usu magma, whose Pb isotopic composition can be considered to
434 be similar to that of Usu#64, represents a mixture of the DMM component and the
435 slab-derived fluid. The mixing ratio of DMM and slab-derived fluid required to produce
436 the primary magma can be estimated using the Pb isotopic compositions of DMM,
437 slab-derived fluid, and the basaltic lavas, as well as the Pb concentrations of DMM and
438 the slab-derived fluid. The Pb isotopic composition and the Pb concentration of the

439 DMM component are assumed to be $^{206}\text{Pb}/^{204}\text{Pb} = 17.65$, $^{207}\text{Pb}/^{204}\text{Pb} = 15.42$,
440 $^{208}\text{Pb}/^{204}\text{Pb} = 37.38$ (Cousens & Allan, 1992; Kuritani *et al.*, 2008), and 0.023ppm
441 (Salters & Stracke, 2004), respectively. It is also assumed that the Pb concentration of
442 the slab fluid was 40 ppm, as estimated for Rishiri volcano in northern Hokkaido (Fig.
443 1; Kuritani *et al.*, 2008). Thus, the relative contribution of the slab-derived fluid to the
444 DMM can be estimated to be ~1%.

445

446 **Degree of melting of the source mantle**

447 The somma basalts are characterized by mostly flat REE patterns from the middle rare
448 earth elements (MREE) to the heavy rare earth elements (HREE) (Fig. 8d). The Gd/Yb
449 ratios of the basalt samples are about 1.3 times that of primitive mantle (PM; Sun &
450 McDonough, 1989), and this relatively low value may be explained by the residence of
451 the source mantle in the spinel stability field. The degree of melting (F) of typical
452 DMM required to produce the primary Usu magma was estimated according to the
453 distribution of Ti between the source mantle and melt using the method of Kelley *et al.*
454 (2006). Using a bulk distribution coefficient for Ti of 0.04 and a TiO_2 content for DMM
455 of 0.133 wt % (Salters & Stracke, 2004), as well as the TiO_2 concentration of the
456 estimated primary magma of 0.50 wt % (Table 2), a degree of melting of 23.1% was
457 obtained. Using the degree of melting of 23.1% and the water content of the estimated

458 primary magma of 3.9 ± 0.39 wt %, the water content of the source mantle can be
459 calculated to be 0.94 ± 0.21 wt % using equation (10) of Kelley *et al.* (2006).

460 The source mantle may have been depleted relative to the DMM of Salters &
461 Stracke (2004) by a previous melt extraction event, and, therefore, the degree of prior
462 melt removal (f) was estimated using the method of Kelley *et al.* (2006). The Ti/Nb
463 ratio of the partial melt is sensitive to f , because the concentrations of more
464 incompatible elements (i.e. Nb) in the source mantle are depleted by a previous melt
465 extraction event more than the concentrations of less incompatible elements (i.e. Ti).
466 The Ti/Nb ratio of Usu#64 is 3980, and this value can be assumed to be that of the
467 primary magma, because this ratio is not affected significantly by the fractionation of
468 olivine. Using a bulk distribution coefficient of 0.04 for Ti and 0.0013 for Nb (Kelley *et*
469 *al.*, 2006) and the Nb and TiO₂ contents of the DMM of Salters & Stracke (2004), the
470 Ti/Nb ratio of ~4000 for the primary Usu magma can be explained by $f = 0.06\%$. This
471 result suggests that the source mantle was not significantly depleted relative to typical
472 DMM.

473

474 **Conditions of generation of Usu magma**

475 The pressure and temperature conditions required to generate a 23.1% partial melt of
476 DMM were calculated for a source water content of 0.94 ± 0.21 wt % using the

477 alphaMELTS model in the pMELTS mode (Ghiorso *et al.*, 2002; Smith & Asimow,
478 2005); results for water contents of 0.73, 0.94, and 1.15 wt % are shown in Fig. 11. In
479 the source mantle, the primary magma was in equilibrium with olivine, and this
480 constraint was also used to estimate the magma generation conditions. The olivine–melt
481 equilibria were examined for the calculated primary melt with a water content of $3.9 \pm$
482 0.9 wt %, using the alphaMELTS model in the pMELTS mode, and the calculated
483 liquidus temperatures as a function of pressure for water contents of 3.0, 3.9, and 4.8
484 wt % (Fig. 11). The temperature and pressure conditions for the generation of the Usu
485 magma that satisfy 23.1% melting of DMM and the equilibration of the melt with
486 olivine in the source mantle are constrained to $1296 \pm 8^\circ\text{C}$ and 1.43 ± 0.10 GPa,
487 respectively (thick gray line in Fig. 11). Beneath Usu volcano, high seismic attenuation
488 is observed at depths of >40 km (Kita *et al.*, 2014). This observation is suggestive of
489 partial melting of the mantle, which is consistent with our estimate of 1.43 ± 0.10 GPa
490 (43–50km depth) for the depth of magma generation.

491

492 **Implications for the nature of the wedge mantle beneath southwestern Hokkaido**

493 In this study, we estimated the temperature and water content of the source mantle to be
494 $1296 \pm 8^\circ\text{C}$ and 0.94 ± 0.21 wt % at a depth corresponding to a pressure of 1.43 ± 0.10
495 GPa. Kuritani *et al.* (2014) estimated the magma generation conditions for Iwate

496 volcano (Fig. 1) and Sannome-gata volcano ('Megata' in Fig. 1), located along an
497 across-strike trend in the NE Japan arc, using an approach essentially similar to that of
498 this study. They showed that the source mantle conditions for the frontal-arc Iwate
499 volcano were 0.6–0.7wt % H₂O at ~1250°C and ~1.3 GPa, and those for the rear-arc
500 Sannome-gata volcano were 0.5–0.6wt % H₂O at 1220–1230°C and ~1.8 GPa. In this
501 case, the temperature of the mantle at ~1.4 GPa was considered to range between
502 ~1230°C and ~1250°C on the across-arc trend, which is significantly lower than the
503 estimated $1296 \pm 8^\circ\text{C}$ at ~1.4 GPa for Usu volcano. The surface of the subducting
504 Pacific slab is continuous at the arc–arc junction beneath Hokkaido, and the presence of
505 a 'slab window' has not been suggested from geophysical studies (Miller *et al.*, 2006;
506 Kennett & Furumura, 2010). Therefore, the higher temperature of the wedge mantle
507 beneath Usu than in the main NE Japan arc may be explained by the wedge mantle at
508 the arc–arc junction not being cooled efficiently by the low-temperature subducting slab,
509 compared with the wedge mantle beneath the main NE Japan arc, because of the
510 bending of the slab at the arc–arc junction. Recently, Wada *et al.* (2015) investigated the
511 mantle wedge flow pattern and the thermal structure for the NE Japan subduction
512 margin (northern part of the NE Japan arc and western part of the Kuril arc) using a
513 numerical approach and suggested that the upper mantle beneath the arc–arc junction is
514 locally cooler than the surrounding region, contrary to the result of our study. According

515 to their modelling the temperature of the mantle at a depth of 50 km beneath Usu
516 volcano is lower than 1050°C. If this were the case, the potential temperature of the
517 primary magmas would be lower than 1000°C. The alphaMELTS model shows that an
518 extremely high water content of >3 wt % would be required to generate ~20% partial
519 melt of DMM mantle under these conditions; in this case, the water content of the
520 primary magma would be more than 15 wt %. These results are not likely to be correct.

521 The water content of the source mantle of 0.94 ± 0.21 wt % for Usu volcano is
522 significantly higher than the 0.6–0.7 wt % determined for Iwate and the 0.5–0.6 wt %
523 content for Sannome-gata. Kimura & Nakajima (2014) also suggested that the water
524 contents of the source mantle for other volcanoes such as Funagata and Chokai, located
525 in the frontal-arc and the rear-arc of the NE Japan arc, respectively, are lower than ~0.3
526 wt % by using the mass-balance model ‘Arc Basalt Simulator version 4’. These
527 observations may suggest that the flux of slab-derived fluids is higher at the arc–arc
528 junction than at the main NE Japan arc. It is widely accepted that subducting oceanic
529 lithosphere is effectively hydrated through the formation of deep normal faults at the
530 outer rise (e.g. Peacock, 2001). Beneath the NE Japan arc–Kurile arc junction, the
531 subducting Pacific plate is distorted (Fig. 1) and normal faults might have formed
532 intensively along the bending part of the slab, in addition to the faulting at the outer rise.
533 It has been suggested that the subducting plate is intensely hydrated at the arc–arc

534 junction beneath southwestern Hokkaido (Garth & Rietbrock, 2014). Consequently,
535 efficient release of fluids from the locally strongly hydrated oceanic plate (Wada *et al.*,
536 2012) may have resulted in the intensive hydration of the overlying mantle wedge.

537

538 **EVOLUTION OF THE SOMMA MAGMAS**

539 The $^{87}\text{Sr}/^{86}\text{Sr}$ ratios of the basaltic andesite samples do not lie on the linear extension of
540 the trend formed by the basaltic lavas in the $^{87}\text{Sr}/^{86}\text{Sr}$ - SiO_2 diagram (Fig. 9a),
541 suggesting that the compositional diversity of the andesitic magmas was produced by
542 different processes than those of the basaltic magmas. Unlike the basaltic lavas, the
543 whole-rock compositions of the basaltic andesite lavas are scattered at a given SiO_2
544 content in Harker diagrams. This observation suggests that the compositional diversity
545 was produced by at least two independent processes that were not coupled to each other.
546 To elucidate the processes responsible for the formation of the compositional diversity,
547 principal component analysis (PCA) was applied to the compositions of the basaltic
548 andesite samples, as well as to those of the three SiO_2 -rich basaltic samples that were
549 not significantly affected by magma mixing.

550 PCA is a procedure that reduces the dimensionality of multivariate data while
551 retaining the maximal amount of variance, and it allows the determination of a new
552 coordinate system consisting of principal components, represented as PC1, PC2, PC3....,

553 in which PC1 explains the maximum variability, PC2 is the next major axis, and so on.
554 In this study, PCA was applied to the major element data (SiO_2 , TiO_2 , Al_2O_3 , Fe_2O_3^* ,
555 MnO , MgO , CaO , Na_2O , K_2O , and P_2O_5 ; i.e. 10 dimensions) for 76 samples. The results
556 of the analysis, including the factors of each element, eigenvalues, explained variances,
557 and cumulative explained variances for PC1, PC2, and PC3, are listed in Table 5. The
558 eigenvalues of PC1, PC2, and PC3 exceed unity; therefore, these components are
559 considered to be significant. The first two components, PC1 and PC2, represent 46.8%
560 and 25.4% of the variance, respectively, and explain more than 70% of the observed
561 variability of the data. The data plotted on PC1–PC2 and PC1–PC3 diagrams are shown
562 in Fig. 12. The basalt samples have relatively higher values of PC1, and these are
563 clearly discriminated from the basaltic andesite samples. The PC1 values of some
564 low- P_2O_5 samples are higher than those of the high- P_2O_5 samples (Fig. 12a). The data
565 for the low- P_2O_5 lavas are discernible from those of the high- P_2O_5 lavas in the
566 PC1–PC3 diagram (Fig. 12b).

567 Many elements, including Al_2O_3 , Fe_2O_3^* , MnO , MgO , Na_2O , and P_2O_5 , make a
568 large contribution to PC1, as suggested by the higher absolute values (>0.3) of the
569 factors of these elements (Table 5). Because P_2O_5 , one of the key elements in the
570 somma lavas, is suggested to be important in PC1 and because the P_2O_5 contents show a
571 good correlation with the $^{206}\text{Pb}/^{204}\text{Pb}$ ratios of the lavas (Fig. 9d), the $^{206}\text{Pb}/^{204}\text{Pb}$ ratios

572 of the lavas are plotted against their PC1 values in Fig. 13a. The figure shows that PC1
573 exhibits a good positive correlation with $^{206}\text{Pb}/^{204}\text{Pb}$, suggesting that PC1 primarily
574 reflects a mixing process between a less radiogenic Pb component and a more
575 radiogenic component.

576 With regard to PC2, the absolute values of the factors of Al_2O_3 and CaO are
577 remarkably high (-0.42 and -0.53 , respectively; Table 5) compared with those of other
578 elements. Considering that these elements are the main components in plagioclase, the
579 relationship between PC2 values and the modal abundances of plagioclase phenocrysts
580 are plotted in Fig. 13b. The contents of the plagioclase phenocrysts show a good
581 correlation with the PC2 values, although the data for the two basaltic samples seem to
582 deviate from the main trend. This observation suggests that PC2 is likely to reflect
583 separation and/or accumulation processes of plagioclase phenocrysts.

584 The oxides TiO_2 , Fe_2O_3^* , CaO, and P_2O_5 have large contributions to PC3.
585 Because TiO_2 and Fe_2O_3^* are the main constituents of titanomagnetite, and CaO and
586 P_2O_5 are the main constituents of apatite, PC3 may reflect magmatic differentiation
587 involving separation of these accessory minerals.

588 With the above considerations, 46.8% of the diversity of the whole-rock major
589 element compositions can be explained by mixing of components with distinct Pb
590 isotopic ratios (PC1), 25.4% of the diversity by redistribution of plagioclase phenocrysts

591 (PC2), and 16.0% by fractionation of accessory minerals (PC3).

592 As suggested above, the compositional diversity of the somma lavas, except for
593 the relatively low-SiO₂ basaltic samples, is largely explained by mixing of a high-SiO₂
594 basaltic magma (high PC1) with high ²⁰⁶Pb/²⁰⁴Pb and another end-member component
595 (low PC1) with low ²⁰⁶Pb/²⁰⁴Pb (Fig. 13a). Considering that the ²⁰⁶Pb/²⁰⁴Pb ratios of the
596 lavas correlate negatively with the whole-rock P₂O₅ contents (Fig. 9d), the low-PC1
597 component must be enriched in P₂O₅; thus, the component is more differentiated and
598 has a lower radiogenic Pb isotopic composition than the basaltic andesite lavas. There
599 are two possibilities for the origin of this low-PC1 component: (1) upper crustal
600 materials; (2) lower crustal materials. The basement rocks, which may constitute the
601 upper crust beneath Usu volcano, belong to the Kitakami Terrane (Ordovician to
602 Cretaceous complex), and some granitoids within the terrane have low ²⁰⁶Pb/²⁰⁴Pb ratios
603 of ~18.4 (e.g. Kimura & Yoshida, 2006). The diorite sample from Kimobetsu has a
604 slightly lower ²⁰⁶Pb/²⁰⁴Pb ratio of 18.49 compared with the Usu somma lavas (>18.5),
605 and this observation is consistent with the postulated less radiogenic Pb characteristics
606 of PC1. However, the ¹⁴³Nd/¹⁴⁴Nd ratios of the granitoids, including the Kimobetsu
607 diorite, are lower than 0.5127 (Kimura & Yoshida, 2006), whereas the low-PC1
608 component is likely to have had a ¹⁴³Nd/¹⁴⁴Nd ratio of ~0.5129, as suggested by the
609 mostly constant ¹⁴³Nd/¹⁴⁴Nd ratios of ~0.5129 of the basaltic andesite lavas (Fig. 9b).

610 For this reason, it is not likely that the low-PC1 component comprises upper crustal
611 materials and we conclude that the component originated from the lower crust.
612 Unfortunately, we do not have samples of the lower crust beneath Usu volcano.
613 However, lower crustal xenoliths from the Ichinome-gata volcano (Fig. 1) have
614 $^{143}\text{Nd}/^{144}\text{Nd}$ ratios of ~ 0.5129 , as well as lower $^{206}\text{Pb}/^{204}\text{Pb}$ ratios than the somma lavas
615 (Table 3; Fig. 10); these data are consistent with the predicted characteristics of the
616 low-PC1 component. Considering that the low-PC1 component is enriched in P_2O_5 , it
617 might have been a relatively low-degree partial melt of the lower crust.

618 High-An plagioclase phenocrysts ($>\text{An}85$) with homogeneous $^{87}\text{Sr}/^{86}\text{Sr}$ are
619 present throughout the somma lavas (Fig. 5), and they are suggested to have formed in
620 the relatively SiO_2 -rich basaltic magmas at 0.65 GPa, as discussed above. Because the
621 depth of the Conrad discontinuity beneath Usu volcano is 18km (Wang & Zhao, 2009),
622 the pressure condition of 0.65 GPa corresponds to a depth in the lower crust. Therefore,
623 the plagioclase phenocrysts are considered to have been present in the basaltic magmas
624 in the lower crust; these then were mixed with partial melts of the lower crust to
625 produce the basaltic andesite magmas.

626 From these considerations, as well as the order of eruption of the somma lavas
627 (i.e. basalt lavas, low- P_2O_5 basaltic andesite lavas, and high- P_2O_5 basaltic andesite
628 lavas), the pre-eruption history of the somma magmas can be summarized as follows. A

629 primary magma, generated at ~1300°C and ~1.4 GPa in the upper mantle, ascended to
630 the lower crust and formed a magma chamber where it then evolved to a SiO₂-rich
631 basalt magma, principally through olivine fractionation. In the magma chamber at a
632 pressure of ~0.65 GPa, high-An plagioclase crystals began to grow, which were
633 followed by crystallization of pyroxenes. This magma was then mixed with another
634 primitive magma with a distinct ⁸⁷Sr/⁸⁶Sr ratio to form the compositional trend of the
635 somma basalt lavas. The SiO₂-rich basalt magmas evolved to basaltic andesitic magmas
636 through mixing with partial melts of the lower crust, followed by differentiation and
637 redistribution of plagioclase phenocrysts in the magma chamber or during magma
638 ascent to the surface.

639

640 **CONCLUSIONS**

641 To investigate the origin of intensive magmatism at an arc–arc junction, we carried out
642 a petrological and geochemical study of mafic lavas from Usu volcano, which is located
643 at the boundary between the NE Japan arc and the Kuril arc. We reached the following
644 conclusions.

645

646 1. The somma lavas of Usu volcano show large variations in geochemistry, and they can
647 be divided into basaltic lavas (49.6–51.3 wt % SiO₂) and basaltic andesite lavas

648 (52.0–54.9 wt % SiO₂).

649 2. The primary magma is estimated to have been generated through ~23% melting of a
650 source mantle with 0.94 ± 0.21 wt % H₂O at $1296 \pm 8^\circ\text{C}$ and 1.43 ± 0.10 GPa. The
651 Pb isotopic composition of the primary magma can be explained by 1% mixing of
652 slab-derived fluid, consisting of a 9:1 mixture of an altered oceanic crust-derived
653 component and a Pacific sediment component, with the depleted MORB-source
654 mantle.

655 3. The estimated water content of 0.94 ± 0.21 wt % for the source mantle beneath Usu
656 volcano is significantly higher than that of the mantle beneath the main part of the
657 NE Japan arc (generally <0.7 wt % H₂O). This observation may suggest that the
658 wedge mantle at the arc–arc boundary is intensively hydrated because of the
659 efficient release of fluids from the slab owing to intensive faulting along the bending
660 part of the Pacific plate.

661 4. The temperature of the wedge mantle at ~1.4 GPa beneath Usu volcano is suggested
662 to be higher than that of the mantle in the main NE Japan arc. This may indicate that
663 the wedge mantle at the arc–arc junction is not cooled efficiently by the
664 low-temperature subducting slab compared with the wedge mantle beneath the main
665 NE Japan arc, because of the bending of the slab at the arc–arc junction.

666 5. Application of principal component analysis to the whole-rock major element

667 compositions of the basaltic andesite lavas suggests that the somma magmas
668 evolved through mixing of a partial melt of the lower crust, followed by
669 differentiation and redistribution of plagioclase phenocrysts in a crustal magma
670 reservoir or during magma ascent to the surface.

671

672

673 **ACKNOWLEDGEMENTS**

674 We thank Mizuho Miyasaka for useful discussion and technical support for geochemical
675 analysis. Yasuo Miyabuchi is also thanked for useful suggestion on Usu volcano. We
676 are grateful to Hidehiko Nomura and Kosuke Nakamura at Hokkaido University for
677 making beautiful thin sections. Editorial handling by John Gamble and constructive
678 review and comments by Georg Zellmer, Anna Volynets, and Martin Streck are greatly
679 appreciated.

680

681 **FUNDING**

682 This work was supported by a research grant from JSPS KAKENHI Grant Numbers
683 25287144 and 25120006 for T.K.

684

685 **SUPPLEMENTARY DATA**

686 Supplementary data for this paper are available at Journal of Petrology online.

687

688

689 **REFERENCES**

- 690 Aoki, K. (1971). Petrology of mafic inclusions from Itinomegata, Japan. *Contributions*
691 *to Mineralogy and Petrology* **30**, 314–331.
- 692 Asimow, P. D. & Ghiorso, M. S. (1998). Algorithmic modifications extending MELTS
693 to calculate subsolidus phase relations. *American Mineralogist* **83**, 1127–1132.
- 694 Cousens, B. L. & Allan, J. F. (1992). A Pb, Sr, and Nd isotopic study of basaltic rocks
695 from the Sea of Japan, LEGS 127/128. In: Tamaki, K., Suyehiro, K., Allan, J. &
696 McWilliams, M. (eds) *Proceedings of the Ocean Drilling Program, Scientific*
697 *Results*, **127–128**. College Station, TX: Ocean Drilling Program, pp. 805–817.
- 698 Dorendorf, F., Wiechert, U. & Wörner, G. (2000). Hydrated subarc mantle: a source for
699 the Kluchevskoy volcano, Kamchatka/Russia. *Earth and Planetary Science*
700 *Letters* **175**, 69–86.
- 701 Ellam, R. M. & Hawkesworth, C. J. (1988). Elemental and isotopic variations in
702 subduction related basalts: evidence for a three component model. *Contributions*
703 *to Mineralogy and Petrology* **98**, 72–80.
- 704 Elliott, T. (2003). Tracers of the slab. In: Eiler, J. (ed.) *Inside the Subduction Factory*.
705 *Geophysical Monograph, American Geophysical Union* **138**, 23–45.
- 706 Fujimaki, H. (1986). Fractional crystallization of the basaltic suite of Usu volcano,
707 southwest Hokkaido, Japan, and its relationships with the associated felsic suite.

708 *Lithos* **19**, 129–140.

709 Garth, T. & Rietbrock, A. (2014). Order of magnitude increase in subducted H₂O due to
710 hydrated normal faults within the Wadati–Benioff zone. *Geology*
711 doi:10.1130/G34730.1.

712 Ghiorso, M. S. & Sack, R. O. (1995). Chemical mass transfer in magmatic processes IV.
713 A revised and internally consistent thermodynamic model for the interpolation
714 and extrapolation of liquid–solid equilibria in magmatic systems at elevated
715 temperatures and pressures. *Contributions to Mineralogy and Petrology* **119**,
716 197–212.

717 Ghiorso, M. S., Hirschmann, M. M., Reiners, P. W. & Kress, V. C. (2002). The
718 pMELTS: A revision of MELTS for improved calculation of phase relations and
719 major element partitioning related to partial melting of the mantle to 3 GPa.
720 *Geochemistry, Geophysics, Geosystems* **3**, 2001GC000217.

721 Honda, S., Yoshida, T. & Aoike, K. (2007). Spatial and temporal evolution of arc
722 volcanism in the northeast Honshu and Izu–Bonin arcs: evidence of small-scale
723 convection under the island arc? *Island Arc* **16**, 214–223.

724 Imai, N., Terashima, S., Itoh, S. & Ando, A. (1995). 1994 compilation values for GSI
725 reference samples, ‘Igneous rock series’. *Geochemical Journal* **29**, 91–95.

726 Ishikawa, T. & Nakamura, E. (1994). Origin of the slab component in arc lavas from

727 across-arc variation of B and Pb isotopes. *Nature* **370**, 205–208.

728 Iwamori, H. (1998). Transportation of H₂O and melting in subduction zones. *Earth and*
729 *Planetary Science Letters* **160**, 65–80.

730 Katsui, Y., Oba, Y., Onuma, K., Suzuki, T., Kondo, Y., Watanabe, T., Niida, K., Uda,
731 T., Hagiwara, S., Nagao, T., Nishikawa, J., Yamamoto, M., Ikeda, Y., Katagawa,
732 H., Tsuchiya, N., Shirahase, M., Nemoto, S., Yokoyama, S., Soya, T., Fujita, T.,
733 Inaba, K. & Koide, K. (1978). Preliminary report of the 1977 eruption of Usu
734 volcano. *Journal of the Faculty of Science, Hokkaido University, Series IV* **18**,
735 385–408.

736 Katsumata, K., Wada, N. & Kasahara, M. (2003). Newly imaged shape of the deep
737 seismic zone within the subducting Pacific plate beneath the Hokkaido corner,
738 Japan–Kurile arc–arc junction. *Journal of Geophysical Research* **108**,
739 doi:10.1029/2002JB002175.

740 Kelley, K. A., Plank, T., Grove, T. L., Stolper, E. M., Newman, S. & Hauri, E. (2006).
741 Mantle melting as a function of water content beneath back-arc basins. *Journal*
742 *of Geophysical Research* **111**, B09208.

743 Kennett, B. L. N. & Furumura, T. (2010). Tears or thinning? Subduction structures in
744 the Pacific plate beneath the Japanese Islands. *Physics of the Earth and*
745 *Planetary Interiors* **180**, 52–58.

746 Kimura, J.-I. & Nakajima, J. (2014). Behaviour of subducted water and its role in
747 magma genesis in the NE Japan arc: a combined geophysical and geochemical
748 approach. *Geochimica et Cosmochimica Acta* **143**, 165–188.

749 Kimura, J.-I. & Yoshida, T. (2006). Contributions of slab fluid, mantle wedge and crust
750 to the origin of Quaternary lavas in the NE Japan Arc. *Journal of Petrology* **47**,
751 2185–2232.

752 Kita, S., Okada, T., Hasegawa, A., Nakajima, J. & Matsuzawa, T. (2010a). Anomalous
753 deepening of a seismic belt in the upper-plane of the double seismic zone in the
754 Pacific slab beneath the Hokkaido corner: Possible evidence for thermal
755 shielding caused by subducted forearc crust materials. *Earth and Planetary
756 Science Letters* **290**, 415–426.

757 Kita, S., Okada, T., Hasegawa, A., Nakajima, J. & Matsuzawa, T. (2010b). Existence of
758 interplane earthquakes and neutral stress boundary between the upper and lower
759 planes of the double seismic zone beneath Tohoku and Hokkaido, northeastern
760 Japan. *Tectonophysics* **496**, 68–82.

761 Kita, S., Nakajima, J., Hasegawa, A., Okada, T., Katsumata, K., Asano, Y. & Kimura, T.
762 (2014). Detailed seismic attenuation structure beneath Hokkaido, northeastern
763 Japan: arc–arc collision process, arc magmatism, and seismotectonics. *Journal
764 of Geophysical Research* **119**, 6486–6511.

- 765 Kuritani, T. & Nakamura, E. (2002). Precise isotope analysis of nanogram-level Pb for
766 natural rock samples without use of double spikes. *Chemical Geology* **186**,
767 31–43.
- 768 Kuritani, T. & Nakamura, E. (2003). Highly precise and accurate isotopic analysis of
769 small amounts of Pb using ^{205}Pb – ^{204}Pb and ^{207}Pb – ^{204}Pb , two double spikes.
770 *Journal of Analytical Atomic Spectrometry* **18**, 1464–1470.
- 771 Kuritani, T., Yokoyama, T. & Nakamura, E. (2008). Generation of rear-arc magmas
772 induced by influx of slab-derived supercritical liquids: implications from alkali
773 basalt lavas from Rishiri Volcano, Kurile arc. *Journal of Petrology* **49**,
774 1319–1342.
- 775 Kuritani, T., Kimura, J.-I., Ohtani, E., Miyamoto, H. & Furuyama, K. (2013). Transition
776 zone origin of potassic basalts from Wudalianchi volcano, northeast China.
777 *Lithos* **156–159**, 1–12.
- 778 Kuritani, T., Yoshida, T., Kimura, J.-I., Takahashi, T., Hirahara, Y., Miyazaki, T.,
779 Senda, R., Chang, Q. & Ito, Y. (2014). Primary melt from Sannome-gata
780 volcano, NE Japan arc: constraints on generation conditions of rear-arc magmas.
781 *Contributions to Mineralogy and Petrology* **167**, 969.
- 782 Lu, Y.-H., Makishima, A. & Nakamura, E. (2007). Coprecipitation of Ti, Mo, Sn and
783 Sb with fluorides and application to determination of B, Ti, Zr, Nb, Mo, Sn, Sb,

784 Hf and Ta by ICP-MS. *Chemical Geology* **236**, 13–26.

785 Machida, H. & Arai, F. (2003). Atlas of Tephra in and around Japan, revised edition.
786 Tokyo: *University of Tokyo Press*, 336 pp. (in Japanese with English abstract).

787 Matsumoto, A. & Nakagawa, M. (2010). Formation and evolution of silicic magma
788 plumbing system: Petrology of the volcanic rocks of Usu volcano, Hokkaido,
789 Japan. *Journal of Volcanology and Geothermal Research* **196**, 185–207.

790 Matsumoto, A., Nakagawa, M. & Nakamura, Y. (2005). Reexamination of the magma
791 plumbing system beneath Usu volcano, Hokkaido, Japan, during the 1663
792 eruption. *Bulletin of Volcanological Society of Japan* **50**, 455–473 (in Japanese,
793 with English abstract).

794 Miller, M. S., Kennett, B. L. N. & Gorbatov, A. (2006). Morphology of the distorted
795 subducted Pacific slab beneath the Hokkaido corner. *Physics of the Earth and*
796 *Planetary Interiors* **156**, 1–11.

797 Miyabuchi, Y., Okuno, M., Torii, M., Yoshimoto, M. & Kobayashi, T. (2014).
798 Tephrostratigraphy and eruptive history of post-caldera stage of Toya Volcano,
799 Hokkaido, northern Japan. *Journal of Volcanology and Geothermal Research*
800 **281**, 34–52.

801 Morishige, M. & van Keken, P. E. (2014). Along-arc variation in the 3-D thermal
802 structure around the junction between the Japan and Kurile arcs. *Geochemistry,*

803 *Geophysics, Geosystems* **15**, 2225–2240.

804 Nakagawa, M. (1992). Spatial variation in chemical composition of Pliocene and
805 Quaternary volcanic rocks in southwestern Hokkaido, northeastern Japan Arc.
806 *Journal of the Faculty of Science, Hokkaido University, Series IV* **23**, 175–197.

807 Nakagawa, M., Ishizuka, Y., Yoshimoto, M., Kudo, T., Aizawa, K., Kitagawa, J.,
808 Hiraga, N., Matsumoto, A., Togari, H., Takahashi, R., Ishii, E., Egusa, M., Seino,
809 H., Amma-Miyasaka, M., Wada, K. & Niida, K. (2002). Eruptive materials of
810 the 2000 eruption of Usu volcano, northern Japan: component materials and
811 their temporal change. *Bulletin of Volcanological Society of Japan* **47**, 279–288
812 (in Japanese, with English abstract).

813 Nakagawa, M., Matsumoto, A., Tajika, J., Hirose, W. & Ohtsu, T. (2005).
814 Re-investigation of eruption history of Usu volcano, Hokkaido, Japan: finding of
815 pre-Meiwa eruption (Late 17th century) between Kanbun (1663) and Meiwa
816 (1769) eruptions. *Bulletin of Volcanological Society of Japan* **50**, 39–52 (in
817 Japanese, with English abstract).

818 Nakajima, J., Shimizu, J., Hori, S. & Hasegawa, A. (2006). Shear-wave splitting
819 beneath the southwestern Kurile arc and northeastern Japan arc: a new insight
820 into mantle return flow. *Geophysical Research Letters* **33**,
821 doi:10.1029/2005GL025053.

- 822 Nakamura, H., Iwamori, H. & Kimura, J.-I. (2008). Geochemical evidence for enhanced
823 fluid flux due to overlapping subducting plates. *Nature Geoscience* **1**, 380–384.
- 824 Noguchi, T., Shinjo, R., Ito, M., Takada, J. & Oomori, T. (2011). Barite geochemistry
825 from hydrothermal chimneys of the Okinawa Trough: insight into chimney
826 formation and fluid/sediment interaction. *Journal of Mineralogical and
827 Petrological Sciences* **106**, 26–35.
- 828 Oba, Y. (1964a). Petrological studies of the Usu volcano, with special reference to
829 somma lavas (I). *Journal of the Japanese Association of Mineralogists,
830 Petrologists and Economic Geologists* **51**, 53–66 (in Japanese with English
831 abstract).
- 832 Oba, Y. (1964b). Petrological studies of the Usu volcano, with special reference to
833 somma lavas (II). *Journal of the Japanese Association of Mineralogists,
834 Petrologists and Economic Geologists* **51**, 88–97 (in Japanese).
- 835 Oba, Y. (1966). Geology and petrology of the Usu volcano, Hokkaido Japan. *Journal of
836 the Faculty of Science, Hokkaido University, Series IV* **13**, 185–236.
- 837 Oba, Y. (1991). Chemical composition of minerals in rocks from Usu volcano,
838 Hokkaido—petrological implications to fractionation of the felsic magma.
839 *Bulletin of Yamagata University, Natural Science* **12**, 355–376 (in Japanese with
840 English abstract).

- 841 Oba, Y., Katsui, Y., Kurasawa, H., Ikeda, Y. & Uda, T. (1983). Petrology of historic
842 rhyolite and dacite from Usu volcano, North Japan. *Journal of the Faculty of*
843 *Science, Hokkaido University, Series IV* **20**, 275–290.
- 844 Oba, Y., Yoshida, T. & Aoki, K. (1985). Geochemistry of Usu volcano, Hokkaido.
845 *Research Report of Laboratory of Nuclear Science, Tohoku University* **18**,
846 189–202 (in Japanese).
- 847 Okumura, K., Soya, T., Ono, K. & Satoh, H. (1981). Petrology of rhyolite and dacite
848 erupted in last 300 years from Usu volcano, Japan. In: Abstracts 1981 IAVCEI
849 Symposium, Tokyo: *Volcanology and Chemistry of the Earth's Interior*, pp.
850 276–277.
- 851 Peacock, S. M. (2001). Are the lower planes of double seismic zones caused by
852 serpentine dehydration in subducting oceanic mantle? *Geology* **29**, 299–302.
- 853 Peacock, S. M. (2003). Thermal structure and metamorphic evolution of subducting
854 slabs. In: Eiler, J. (ed.) *Inside the Subduction Factory. Geophysical Monograph,*
855 *American Geophysical Union* **138**, 7–22.
- 856 Peacock, S. M. & Wang, K. (1999). Seismic consequences of warm versus cool
857 subduction metamorphism: Examples from southwest and northeast Japan.
858 *Science* **286**, 937–939.
- 859 Pin, C. & Zalduegui, J. F. S. (1997). Sequential separation of light rare-earth elements,

860 thorium and uranium by miniaturized extraction chromatography: application to
861 isotopic analyses of silicate rocks. *Analytica Chimica Acta* **339**, 79–89.

862 Pin, C., Briot, D., Bassin, C. & Poitrasson, F. (1994). Concomitant separation of
863 strontium and samarium–neodymium for isotopic analysis in silicate samples,
864 based on specific extraction chromatography. *Analytica Chimica Acta* **298**,
865 209–217.

866 Putirka, K. D. (2008). Thermometers and barometers for volcanic systems. In: Putirka,
867 K. D. & Tepley, F. J., III (eds) *Minerals, Inclusions and Volcanic Processes*.
868 *Mineralogical Society of America and Geochemical Society, Reviews in*
869 *Mineralogy and Petrology* **69**, 61–120.

870 Righter, K., Chesley, J. T., Caiazza, C. M., Gibson, E. K. & Ruiz, J. (2008). Re and Os
871 concentrations in arc basalts: the roles of volatility and source region fO₂
872 variations. *Geochimica et Cosmochimica Acta* **72**, 926–947.

873 Ringwood, A. E. (1974). The petrological evolution of island arc systems. *Journal of*
874 *the Geological Society, London* **130**, 183–204.

875 Sakuyama, M. & Nesbitt, R. W. (1986). Geochemistry of the Quaternary volcanic rocks
876 of the northeast Japan arc. *Journal of Volcanology and Geothermal Research* **29**,
877 413–450.

878 Salters, V. J. M. & Stracke, A. (2004). Composition of the depleted mantle.

- 879 *Geochemistry, Geophysics, Geosystems* **5**, Q05B07.
- 880 Smith, P. M. & Asimow, P. D. (2005). Adibat_1ph: a new public front-end to the
881 MELTS, pMELTS, and pHMELTS models. *Geochemistry, Geophysics,*
882 *Geosystems* **6**, 2004GC000816.
- 883 Soya, T., Katsui, Y., Niida, K. & Sakai, K. (1981). Geological Map of Usu Volcano,
884 1:25000. Tsukuba: *Geological Survey of Japan* (in Japanese with English
885 abstract).
- 886 Soya, T., Katsui, Y., Niida, K., Sakai, K. & Tomiya, A. (2007). Geological map of Usu
887 Volcano, 1:25000, 2nd edn. Geological Map of Volcanoes 2. Tsukuba:
888 *Geological Survey of Japan* (in Japanese with English abstract).
- 889 Suda, Y., Okudaira, T. & Furuyama, K. (2010). X-ray fluorescence (XRF; RIX-2100)
890 analysis of major and trace elements for silicate rocks by low dilution glass bead
891 method. *Magma* **92**, 21–39 (in Japanese).
- 892 Sun, S.-S. & McDonough, W. F. (1989). Chemical and isotopic systematics of oceanic
893 basalts: implications for mantle composition and processes. In: Saunders, A. D.
894 & Norry, M. J. (eds) *Magmatism in the Ocean Basins*. *Geological Society,*
895 *London, Special Publications* **42**, 313–345.
- 896 Tamura, Y., Tatsumi, Y., Zhao, D., Kido, Y. & Shukuno, H. (2002). Hot fingers in the
897 mantle wedge: new insights into magma genesis in subduction zones. *Earth and*

- 898 *Planetary Science Letters* **197**, 105–116.
- 899 Tatsumi, Y. (1986). Formation of the volcanic front in subduction zones. *Geophysical*
900 *Research Letters* **13**, 717–720.
- 901 Tatsumi, Y. (1989). Migration of fluid phases and genesis of basalt magmas in
902 subduction zones. *Journal of Geophysical Research* **94**, 4697–4707.
- 903 Tatsumi, Y., Sakuyama, M., Fukuyama, H. & Kushiro, I. (1983). Generation of arc
904 basalt magmas and thermal structure of the mantle wedge in subduction zones.
905 *Journal of Geophysical Research* **88**, 5815–5825.
- 906 Tomiya, A. & Takahashi, E. (1995). Reconstruction of an evolving magma chamber
907 beneath Usu Volcano since the 1663 eruption. *Journal of Petrology* **36**,
908 617–636.
- 909 Tomiya, A. & Takahashi, E. (2005). Evolution of the magma chamber beneath Usu
910 volcano since 1663: a natural laboratory for observing changing phenocryst
911 compositions and textures. *Journal of Petrology* **46**, 2395–2426.
- 912 Tomiya, A., Takahashi, E., Furukawa, N. & Suzuki, T. (2010). Depth and evolution of a
913 silicic magma chamber: melting experiments on a low-K rhyolite from Usu
914 Volcano, Japan. *Journal of Petrology* **51**, 1333–1354.
- 915 van Keken, P. E., Kiefer, B. & Peacock, S. M. (2002). High-resolution models of
916 subduction zones: implications for mineral dehydration reactions and the

917 transport of water into the deep mantle. *Geochemistry, Geophysics, Geosystems*
918 **3**, 2001GC000256.

919 Wada, I., Behn, M. D. & Shaw, A. M. (2012). Effects of heterogeneous hydration in the
920 incoming plate, slab rehydration, and mantle wedge hydration on slab-derived
921 H₂O flux in subduction zones. *Earth and Planetary Science Letters* **353–354**,
922 60–71.

923 Wada, I., He, J., Hasegawa, A. & Nakajima, J. (2015). Mantle wedge flow pattern and
924 thermal structure in Northeast Japan: effects of oblique subduction and 3-D slab
925 geometry. *Earth and Planetary Science Letters* **426**, 76–88.

926 Wang, Z. & Zhao, D. (2005). Seismic imaging of the entire arc of Tohoku and
927 Hokkaido in Japan using P-wave, S-wave and sP depth-phase data. *Physics of*
928 *the Earth and Planetary Interiors* **152**, 144–162.

929 Wang, J. & Zhao, D. (2009). P-wave anisotropic tomography of the crust and upper
930 mantle under Hokkaido, Japan. *Tectonophysics* **469**, 137–149.

931 White, W. M. & Dupré, B. (1986). Sediment subduction and magma genesis in the
932 Lesser Antilles: isotopic and trace element constraints. *Journal of Geophysical*
933 *Research* **91**, 5927–5941.

934 Yokoyama, I., Katsui, Y., Oba, Y. & Ehara, Y. (1973). Usu-volcano, its volcanic
935 geology, history of eruptions, present state of activity and prevention of disasters.

- 936 Sapporo: *Committee for the Prevention of Disasters of Hokkaido*, 254 pp. (in
937 Japanese).
- 938 Yokoyama, T., Makishima, A. & Nakamura, E. (1999). Evaluation of the
939 coprecipitation of incompatible trace elements with fluoride during silicate rock
940 dissolution by acid digestion. *Chemical Geology* **157**, 175–187.
- 941 Zindler, A. & Hart, S. (1986). Chemical geodynamics. *Annual Review of Earth and*
942 *Planetary Science* **14**, 493–571.
- 943
- 944

945 **Figure captions**

946 Fig. 1: Map showing the locations of the active volcanoes in NE Japan. Thin grey
947 dashed lines denote slab surface depth contours, and open triangles indicate the
948 locations of active volcanoes. The location of Usu volcano and those of Megata
949 (Ichinome-gata and Sannome-gata), Iwate, and Rishiri volcanoes are also shown (note
950 that the Megata volcanoes are not active volcanoes). The slab surface depth contours
951 and the subduction direction are from Kita et al. (2010b).

952

953 Fig. 2: Map showing the location of Usu volcano (inset) and geological map of the
954 volcano showing sampling localities (after Matsumoto & Nakagawa, 2010). The
955 location of the inset map is shown in Fig. 1.

956

957 Fig. 3: Photomicrographs of representative samples of (a) a lower-SiO₂ basalt lava
958 (Usu#10), (b) a higher-SiO₂ basalt lava (Usu#64), (c) a low-P₂O₅ basaltic andesite lava
959 (Usu#47a), and (d) a high-P₂O₅ basaltic andesite lava (Usu#48). The horizontal scale
960 bar represents 1mm. ol, olivine; cpx, clinopyroxene; opx, orthopyroxene.

961

962 Fig. 4: Histogram of the Mg# of the cores of olivine phenocrysts in the lower-SiO₂
963 basalt sample (Usu#10) (one datum for each phenocryst).

964

965 Fig. 5: Histograms of the An contents of the cores of plagioclase phenocrysts in basalt,
966 low-P₂O₅ basaltic andesite and high-P₂O₅ basaltic andesite (one datum for each
967 phenocryst).

968

969 Fig. 6: Relationship between the An content of plagioclase phenocrysts and the Mg# of
970 coexisting pyroxene phenocrysts (showing evidence of simultaneous growth in the same
971 crystal aggregates) in the somma lavas.

972

973 Fig. 7: SiO₂ variation diagrams for TiO₂, Al₂O₃, MgO, CaO, K₂O, and P₂O₅ in the
974 somma lavas from Usu volcano.

975

976 Fig. 8: SiO₂ variation diagrams for (a) Ni, (b) Sr, and (c) Y; (d) primitive
977 mantle-normalized trace element patterns of the somma lavas (symbols as in Fig. 7).
978 Trace element concentrations of primitive mantle are from Sun & McDonough (1989).

979

980 Fig. 9: SiO₂ variation diagrams for (a) ⁸⁷Sr/⁸⁶Sr, (b) ¹⁴³Nd/¹⁴⁴Nd, and (c) ²⁰⁶Pb/²⁰⁴Pb; (d)
981 ²⁰⁶Pb/²⁰⁴Pb vs P₂O₅ (symbols as in Fig. 7). In (a), the range of the ⁸⁷Sr/⁸⁶Sr ratios of the
982 plagioclase phenocrysts is shown.

983

984 Fig. 10: Sr, Nd, and Pb isotopic compositions of somma lavas from Usu volcano, along
985 with those of a diorite sample from Kimobetsu and hornblende gabbro xenoliths from
986 Ichinomegata, shown in $^{143}\text{Nd}/^{144}\text{Nd}$ – $^{87}\text{Sr}/^{86}\text{Sr}$ and $^{208}\text{Pb}/^{204}\text{Pb}$ – $^{206}\text{Pb}/^{204}\text{Pb}$ diagrams.
987 The compositional field of DMM is from Zindler & Hart (1986), and those of Pacific
988 MORB and Pacific sediments are from Kimura & Yoshida (2006). In (b) representative
989 compositions (open crosses) of the Pacific sediments and Pacific MORB are taken from
990 Kimura & Nakajima (2014), and that of DMM from Cousens & Allan (1992).

991

992 Fig. 11: Estimated generation conditions for the Usu primary magmas. The P–T
993 conditions of the source mantle required to generate 23.1% partial melt with a source
994 water content of 0.94 ± 0.21 wt % (0.73, 0.94, and 1.15 wt %) and the liquidus
995 temperature of olivine for a primary magma with a water content of 3.9 ± 0.9 wt % (3.0,
996 3.9, and 4.8 wt %), calculated using the alphaMELTS model, are shown with dashed
997 lines and continuous lines, respectively. The thick gray line shows the P–T conditions of
998 magma generation that satisfy the two conditions that (1) degree of melting is 23.1%,
999 and (2) the primary melt was in equilibrium with olivine. The filled circle indicates the
1000 most plausible conditions under which the primary magmas were generated. It should
1001 be noted that orthopyroxene and clinopyroxene become liquidus phases, instead of

1002 olivine, at >1.4–1.5 GPa for the primary melt.

1003

1004 Fig. 12: The compositional data of the 73 basaltic andesite and three basalt samples in

1005 (a) a PC2–PC1 diagram and (b) a PC3– PC1 diagram.

1006

1007 Fig. 13: (a) $^{206}\text{Pb}/^{204}\text{Pb}$ ratios of the samples plotted versus PC1 and (b) the modal

1008 abundance of plagioclase phenocrysts plotted versus PC2.

Table 1 Phenocryst contents of the representative somma samples from Usu Volcano

Sample#	Type	SiO ₂ wt. %	Ol	Opx	Cpx	Pl
Usu#10	Basalt	49.7	8.1	5.2	0.2	16.1
Usu#9a	Basalt	50.0	6.1	0.2	2.2	16.7
Usu#65	Basalt	50.7	2.0	0.4	Tr.	9.8
Usu#47b	Basalt	50.9	0.8	3.7	2.2	18.9
Usu#64	Basalt	51.3	0.1	7.3	1.6	26.1
Usu#47a	Low-P ₂ O ₅ basaltic andesite	52.9	0.3	10.2	3.3	18.5
Usu#16	Low-P ₂ O ₅ basaltic andesite	54.2	-	4.7	2.3	32.3
Usu#55	Low-P ₂ O ₅ basaltic andesite	54.7	-	1.8	0.7	20.7
Usu#23	High-P ₂ O ₅ basaltic andesite	52.8	-	1.6	Tr.	20.8
Usu#2	High-P ₂ O ₅ basaltic andesite	53.2	0.3	6.9	0.3	20.8
Usu#48	High-P ₂ O ₅ basaltic andesite	54.9	-	0.4	Tr.	15.4

Ol: olivine, Opx: orthopyroxene, Cpx: clinopyroxene, Pl: plagioclase, Tr.: Trace

Table 2: Whole-rock compositions of somma lavas from Usu Volcano

Sample:	Usu#2	Usu#9a	Usu#10	Usu#16	Usu#18	Usu#36a	Usu#48	Usu#55	Usu#64	Mrtk#1	Usu#64 ^{a,b}
Type	High-P ₂ O ₅	Basalt	Basalt	Low-P ₂ O ₅	High-P ₂ O ₅	Low-P ₂ O ₅	High-P ₂ O ₅	Low-P ₂ O ₅	Basalt	Diorite	
<i>Major elements (wt %)</i>											
SiO ₂	53.51	49.99	49.72	54.09	52.28	52.51	54.77	54.72	51.43	59.30	49.24
TiO ₂	0.86	0.67	0.67	0.67	0.82	0.71	0.89	0.71	0.62	0.85	0.50
Al ₂ O ₃	18.75	18.69	18.13	20.21	19.57	17.75	18.26	18.52	18.21	16.78	14.73
Fe ₂ O ₃ ^{*a}	10.53	11.59	12.03	8.79	10.41	11.08	10.42	9.80	10.95	7.46	11.09
MnO	0.18	0.20	0.21	0.17	0.18	0.19	0.18	0.17	0.19	0.14	0.15
MgO	3.56	6.66	7.38	3.07	3.88	5.10	2.69	3.33	6.10	4.18	14.04
CaO	9.77	9.74	9.75	9.63	10.13	9.31	8.79	9.38	10.10	5.85	8.17
Na ₂ O	2.75	1.89	1.86	2.60	2.73	2.23	3.14	2.63	2.13	3.08	1.73
K ₂ O	0.49	0.22	0.23	0.45	0.42	0.42	0.52	0.64	0.36	2.09	0.29
P ₂ O ₅	0.17	0.07	0.07	0.12	0.12	0.10	0.15	0.10	0.08	0.14	0.06
Total	100.56	99.72	100.05	99.80	100.54	99.39	99.81	100.00	100.16	99.86	4.14
LOI	-0.47	0.41	-0.01	0.17	-0.51	0.52	-0.36	0.02	0.24	0.44	-
<i>Trace elements (ppm)</i>											
V (XRF)	275	256	276	187	261	267	243	248	245	175	-
Cr (XRF)	26.0	33.8	38.8	8.75	28.7	44.4	7.64	12.8	51.7	44.0	-
Ni (XRF)	16.9	38.1	50.9	8.43	20.4	14.3	2.51	5.85	25.3	23.9	-
Rb	6.82	3.26	3.53	6.79	5.78	7.25	5.87	11.81	5.58	97.08	-
Sr	367	346	326	383	389	324	365	344	331	306	-
Y	21.7	12.4	12.9	18.2	18.3	17.7	17.6	20.6	14.3	15.2	-
Zr	50.1	28.1	25.7	47.1	39.8	43.6	41.7	49.0	32.2	4.3	-
Nb	1.80	0.74	0.70	1.32	1.32	1.44	1.21	1.61	0.93	8.03	-
Cs	0.50	0.32	0.39	0.54	0.29	0.58	0.38	0.73	0.21	3.54	-
Ba	228	120	119	195	206	197	181	239	157	364	-
La	6.47	2.35	2.64	4.77	4.83	4.62	4.53	6.11	3.42	12.36	-
Ce	16.6	6.31	6.74	12.0	11.9	11.5	11.9	15.4	8.56	25.94	-
Pr	2.27	0.92	0.99	1.69	1.70	1.64	1.61	2.06	1.25	3.61	-
Nd	11.0	4.72	5.11	8.26	8.43	7.93	7.93	9.67	6.20	14.71	-
Sm	3.08	1.51	1.61	2.42	2.52	2.32	2.33	2.73	1.88	3.30	-
Eu	1.04	0.60	0.63	0.86	0.92	0.78	0.81	0.87	0.67	0.83	-
Gd	3.68	1.94	2.10	2.96	3.06	2.86	2.87	3.31	2.35	3.37	-
Tb	0.61	0.33	0.36	0.50	0.52	0.48	0.49	0.55	0.41	0.54	-
Dy	4.08	2.30	2.48	3.36	3.50	3.28	3.30	3.73	2.76	3.49	-
Ho	0.87	0.50	0.54	0.73	0.75	0.71	0.70	0.81	0.59	0.72	-
Er	2.61	1.52	1.64	2.21	2.25	2.15	2.13	2.47	1.79	2.18	-
Tm	0.38	0.23	0.24	0.33	0.33	0.32	0.32	0.37	0.27	0.32	-
Yb	2.62	1.54	1.66	2.24	2.24	2.17	2.18	2.49	1.85	2.20	-
Lu	0.40	0.24	0.26	0.35	0.34	0.33	0.33	0.38	0.28	0.33	-
Hf	1.61	0.94	0.87	1.51	1.28	1.44	1.34	1.53	1.06	0.37	-
Ta	0.09	0.04	0.04	0.07	0.07	0.08	0.07	0.09	0.05	0.75	-
Pb	6.84	4.32	4.20	6.64	6.53	5.90	5.38	7.04	3.80	6.91	-
Th	0.75	0.31	0.32	0.66	0.60	0.72	0.59	1.10	0.45	2.10	-
U	0.27	0.12	0.12	0.24	0.23	0.27	0.22	0.38	0.18	1.29	-
<i>Isotope</i>											
⁸⁷ Sr/ ⁸⁶ Sr	0.703894±7	0.703835±15	0.703846±15	0.703845±10	0.703879±15	0.703798±15	0.703866±8	0.703810±10	0.703808±14	0.704912±15	-
¹⁴³ Nd/ ¹⁴⁴ Nd	0.512897±16	0.512918±9	0.512900±9	0.512908±13	0.512914±7	0.512931±8	0.512909±13	0.512901±15	0.512898±12	0.512699±9	-
²⁰⁶ Pb/ ²⁰⁴ Pb	18.5311±5	18.6208±8	18.6294±7	18.5869±7	18.5569±8	18.5868±6	18.5543±7	18.5613±5	18.5993±4	18.4858±4	-
²⁰⁷ Pb/ ²⁰⁴ Pb	15.5721±6	15.5719±8	15.5750±8	15.5730±7	15.5709±6	15.5751±6	15.5758±6	15.5719±5	15.5731±4	15.5909±4	-
²⁰⁸ Pb/ ²⁰⁴ Pb	38.5321±16	38.5844±21	38.5966±21	38.5661±21	38.5439±19	38.5717±17	38.5550±19	38.5492±16	38.5753±14	38.5838±10	-

^a Fe₂O₃*: total Fe as Fe₂O₃.^b Estimated primary magma composition for Usu#64
Errors on isotope ratios are within-run 2SE.

Table 3 Isotopic ratios of lower crustal xenoliths from Ichinome-gata

Sample	$^{87}\text{Sr}/^{86}\text{Sr}$	$^{143}\text{Nd}/^{144}\text{Nd}$	$^{206}\text{Pb}/^{204}\text{Pb}$	$^{207}\text{Pb}/^{204}\text{Pb}$	$^{208}\text{Pb}/^{204}\text{Pb}$
IX-1	0.704784±10	-	18.4061±5	15.5644±6	38.4335±17
IX-2	0.704204±15	0.512875±8	18.5149±3	15.5548±4	38.4732±10

Table 4 $^{87}\text{Sr}/^{86}\text{Sr}$ ratios of separates of plagioclase phenocrysts from Usu#10, Usu#16, and Usu#64

Sample	$^{87}\text{Sr}/^{86}\text{Sr}$
Usu#10-p11	0.703805±9
Usu#10-p12	0.703804±8
Usu#10-p13	0.703798±11
Usu#10-p14	0.703796±11
Usu#16-p11	0.703795±11
Usu#16-p12	0.703812±10
Usu#16-p13	0.703791±9
Usu#16-p14	0.703807±10
Usu#64-p11	0.703806±14
Usu#64-p12	0.703811±15
Usu#64-p13	0.703792±7
Usu#64-p14	0.703812±8

Table 5 Result of the principal component analysis for the somma lavas

	PC1	PC2	PC3
Factors			
SiO ₂	-0.20	0.41	-0.45
TiO ₂	-0.22	0.27	0.59
Al ₂ O ₃	-0.32	-0.42	-0.12
Fe ₂ O ₃ *	0.32	0.27	0.43
MnO	0.40	0.22	0.03
MgO	0.43	-0.11	0.03
CaO	-0.12	-0.53	0.22
Na ₂ O	-0.40	0.21	0.04
K ₂ O	-0.24	0.36	-0.13
P ₂ O ₅	-0.36	0.03	0.42
Eigenvalue	4.68	2.54	1.60
Explained variance, %	0.47	0.25	0.16
Cumulative explained variance, %	0.47	0.72	0.88

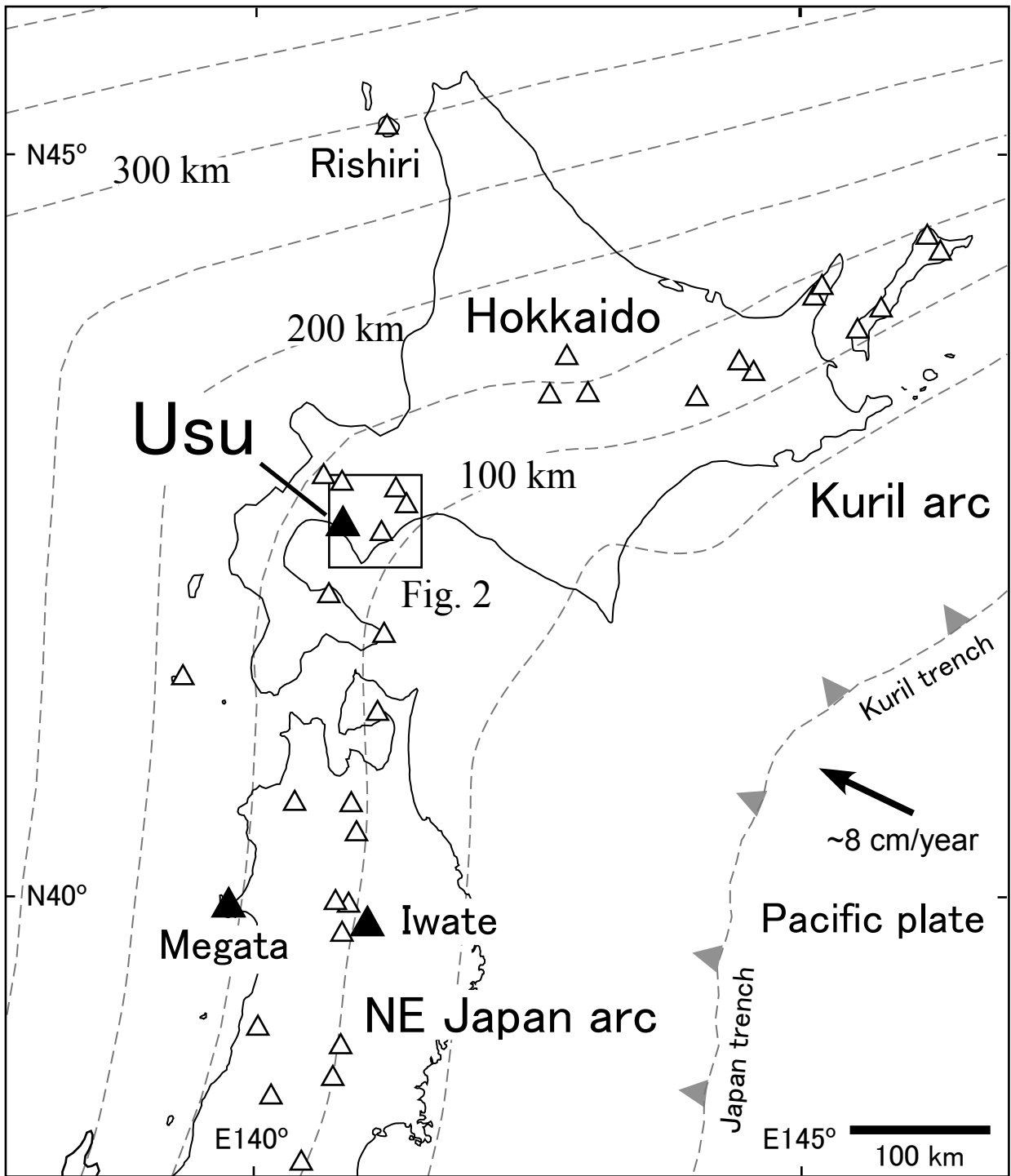


Figure 1

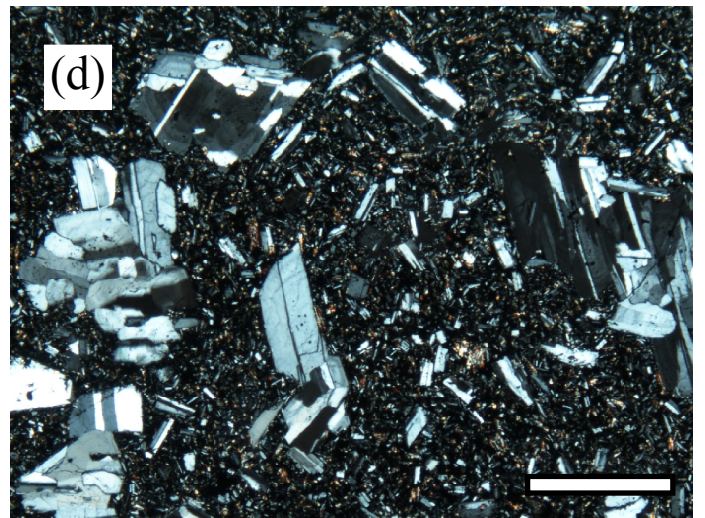
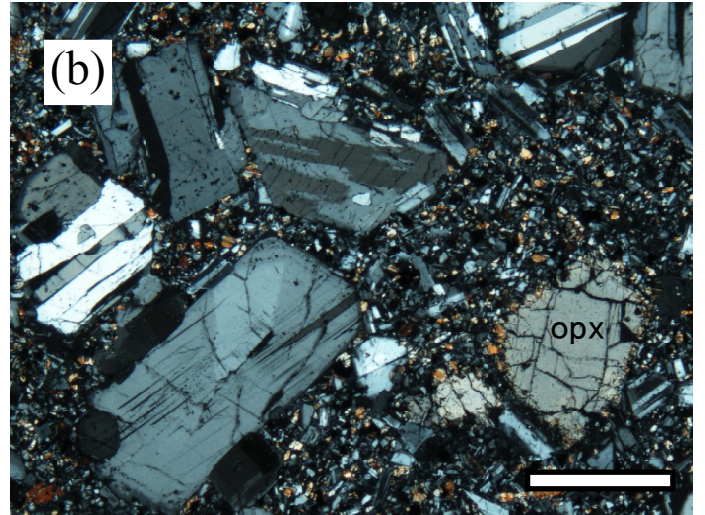
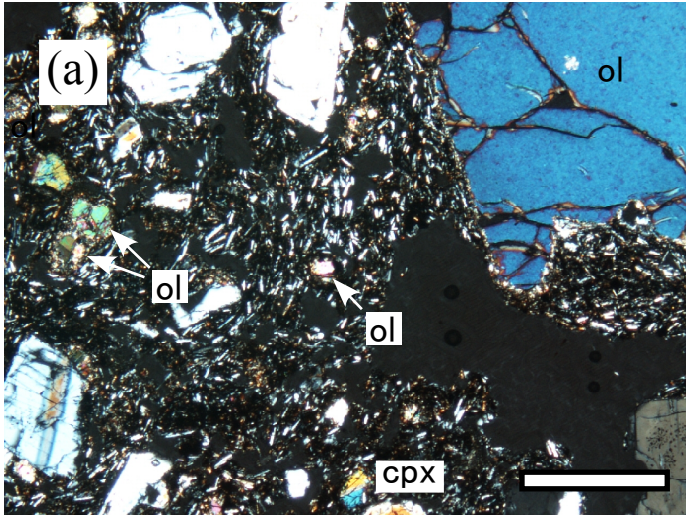


Figure 3

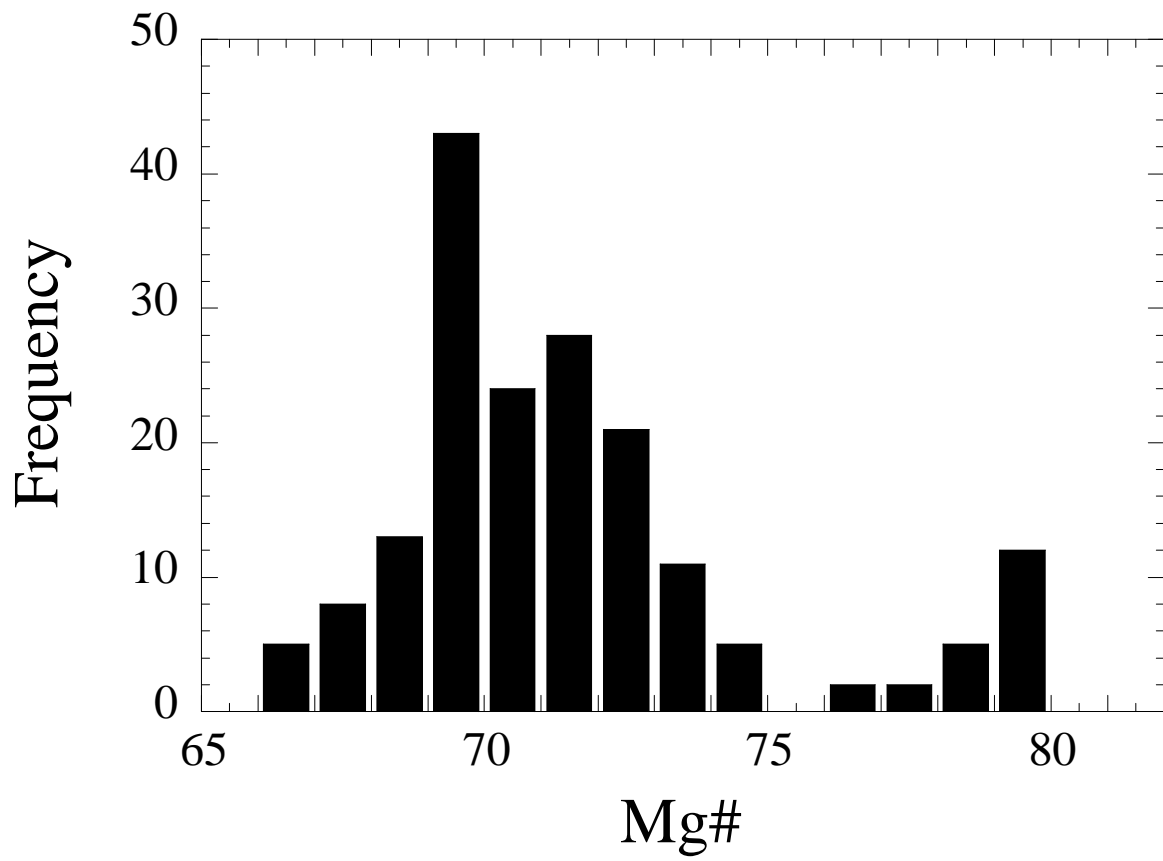


Figure 4

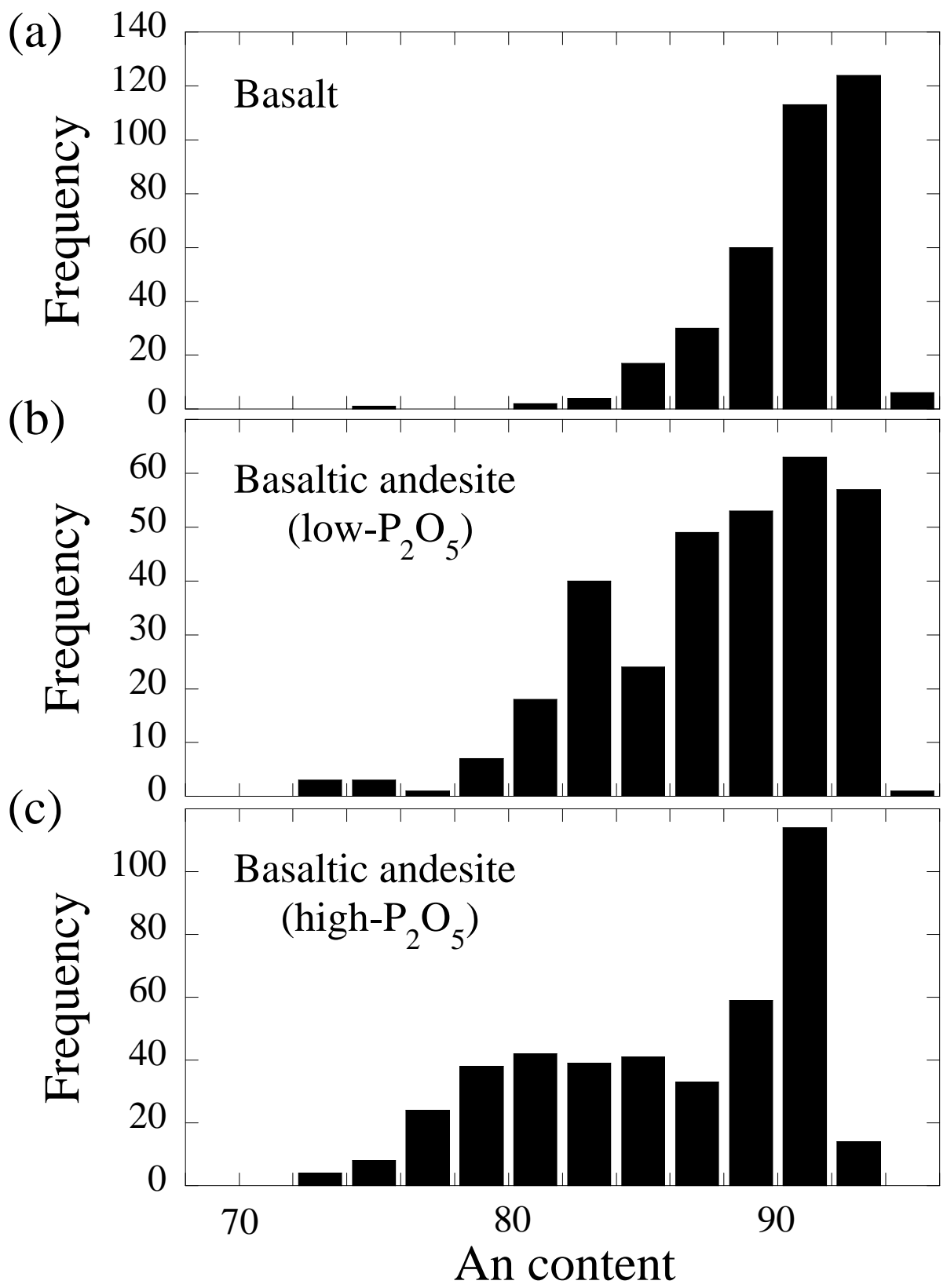


Figure 5

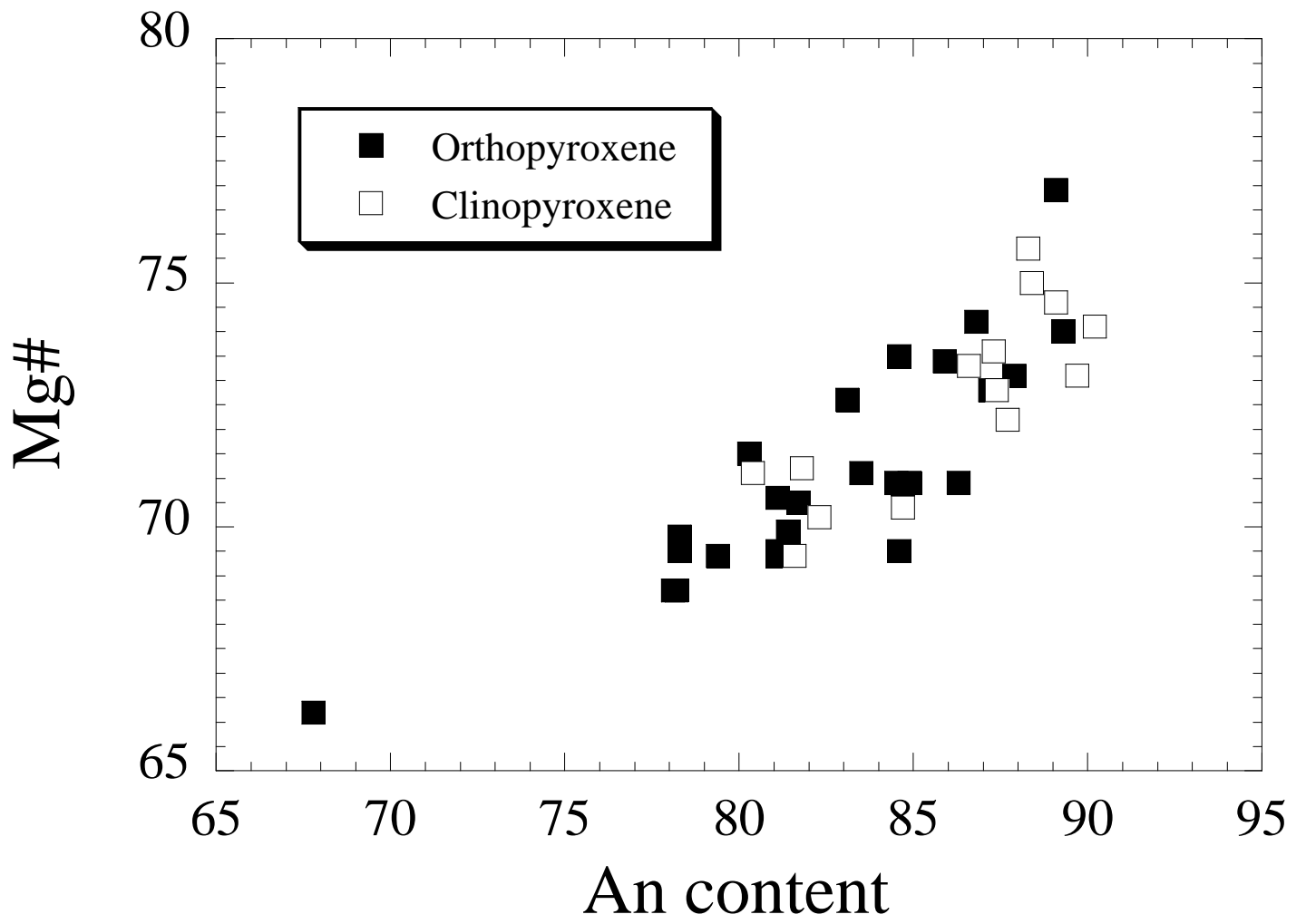


Figure 6

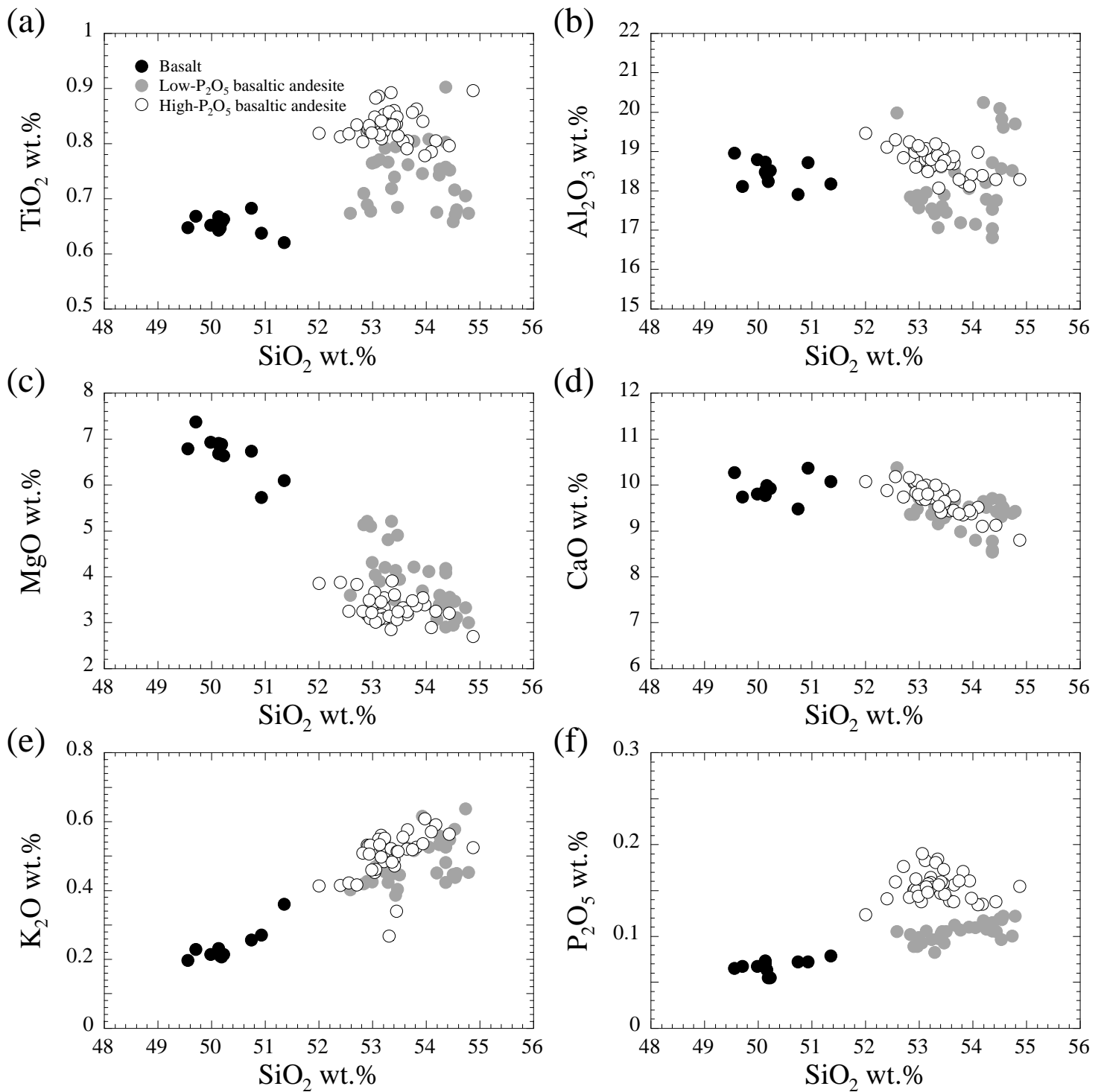


Figure 7

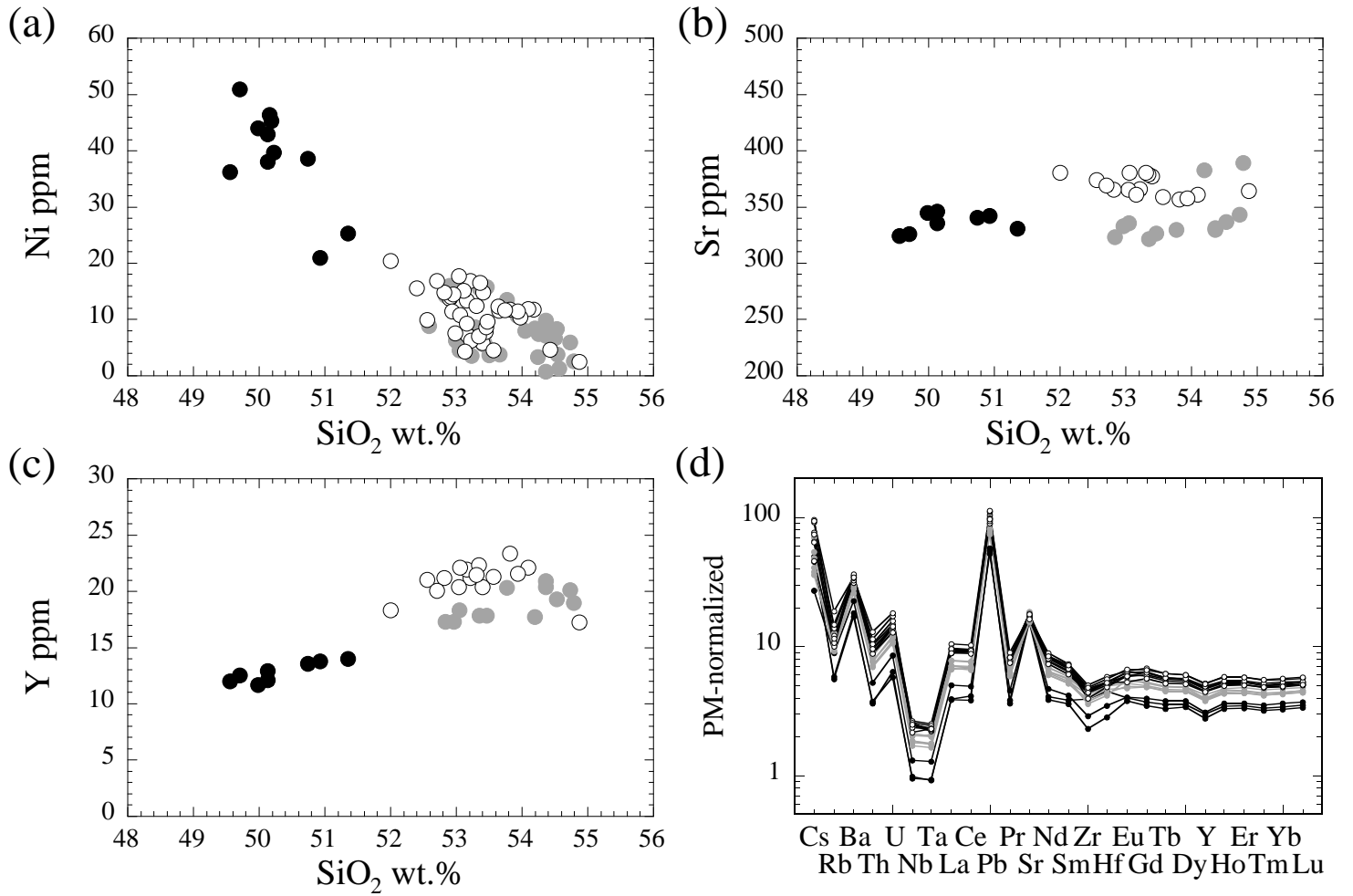


Figure 8

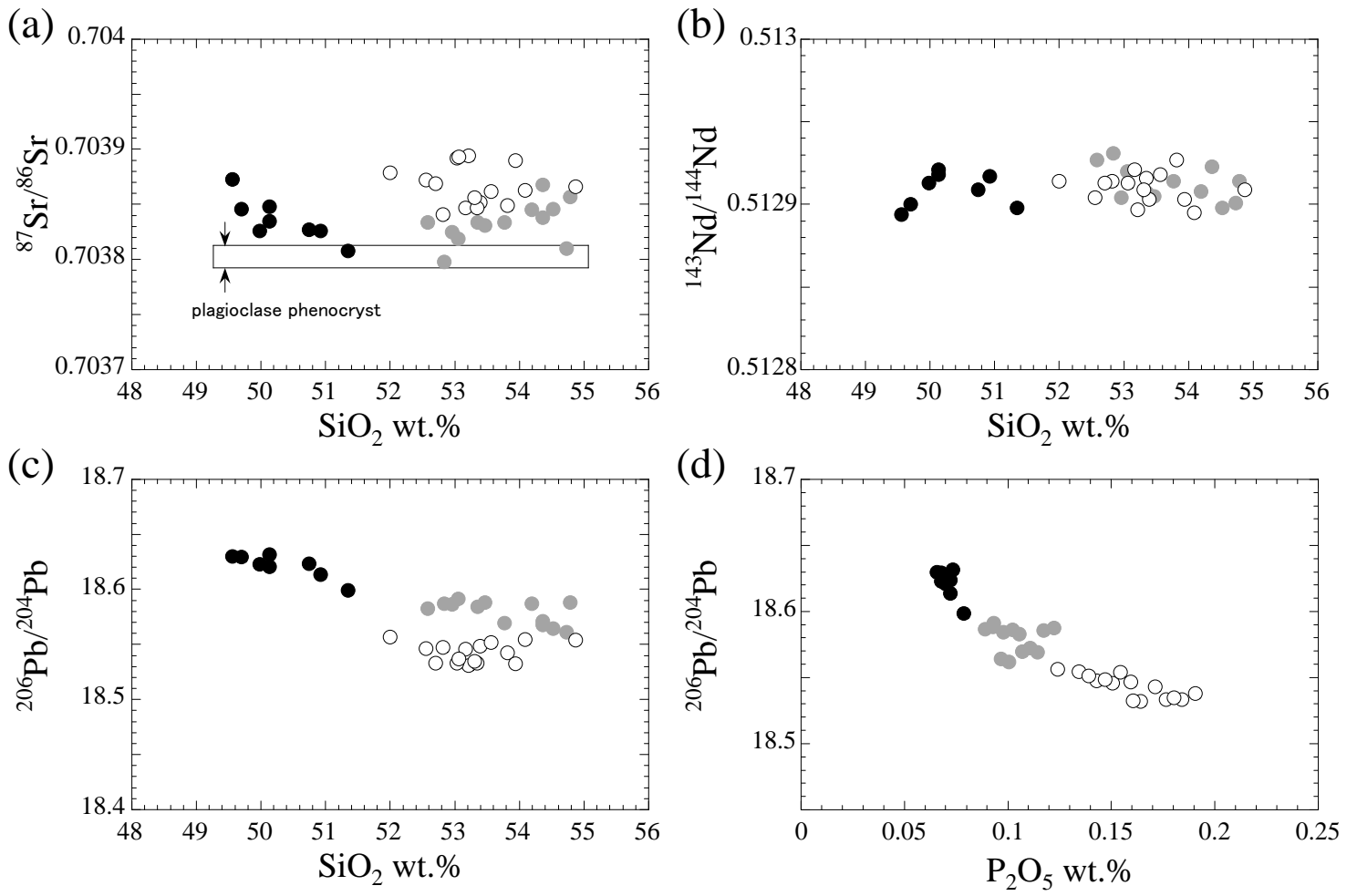


Figure 9

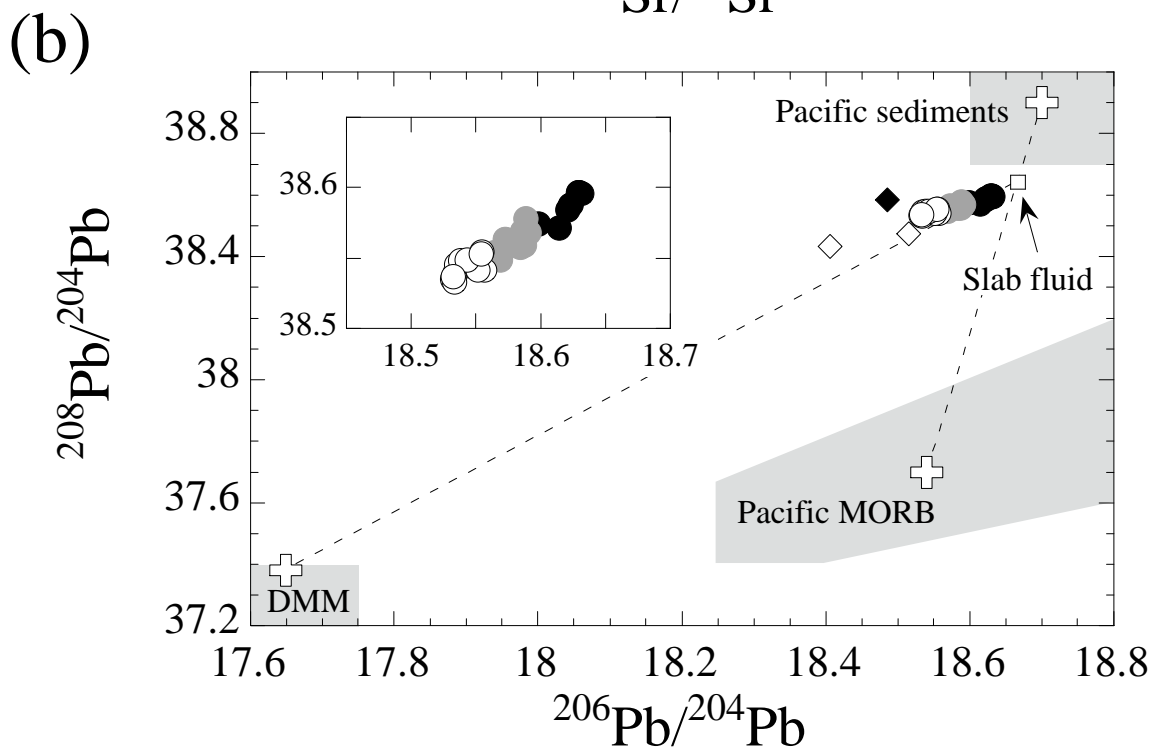
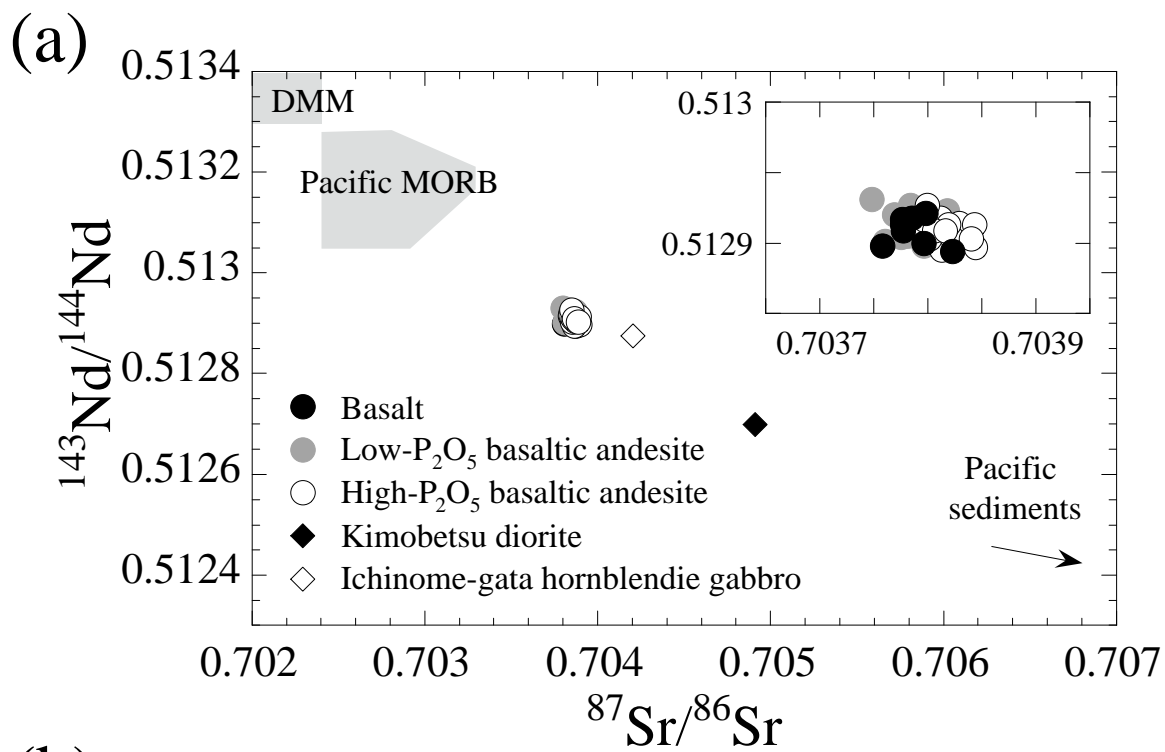


Figure 10

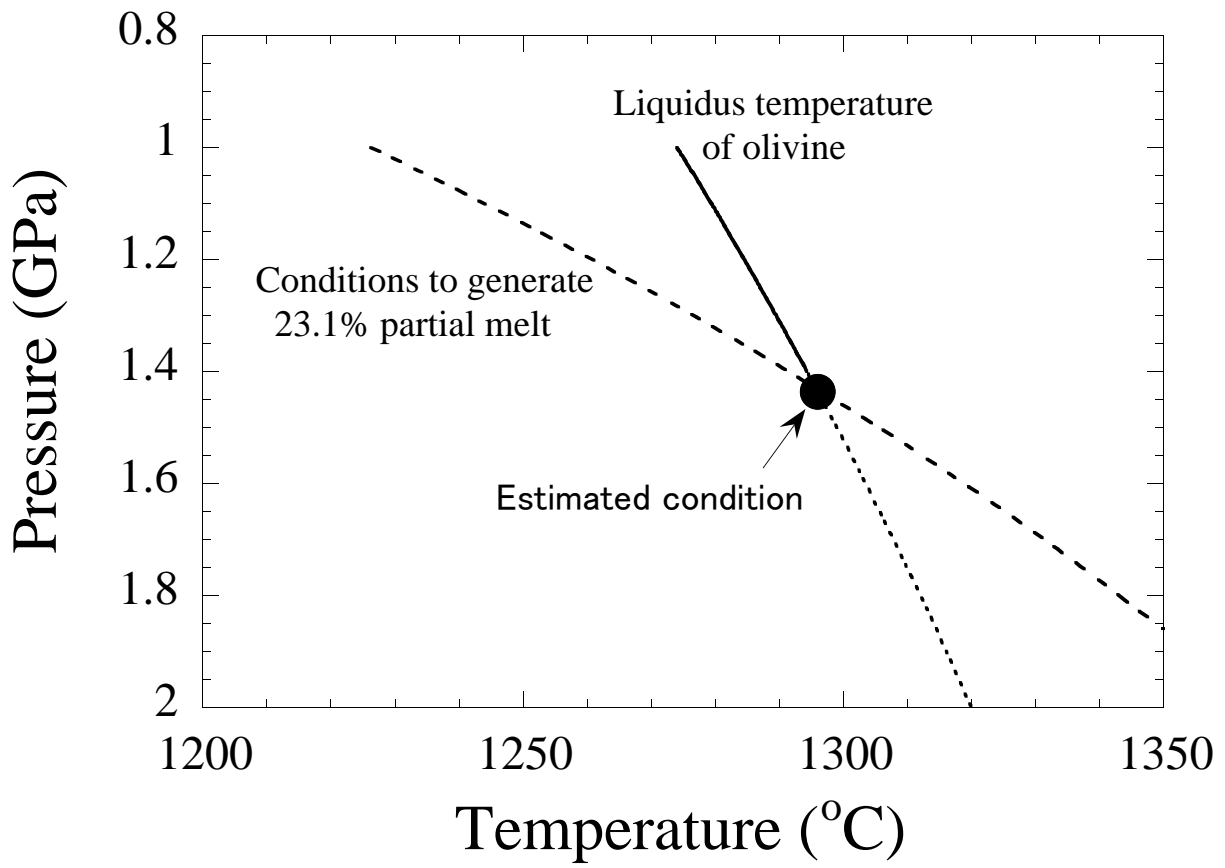
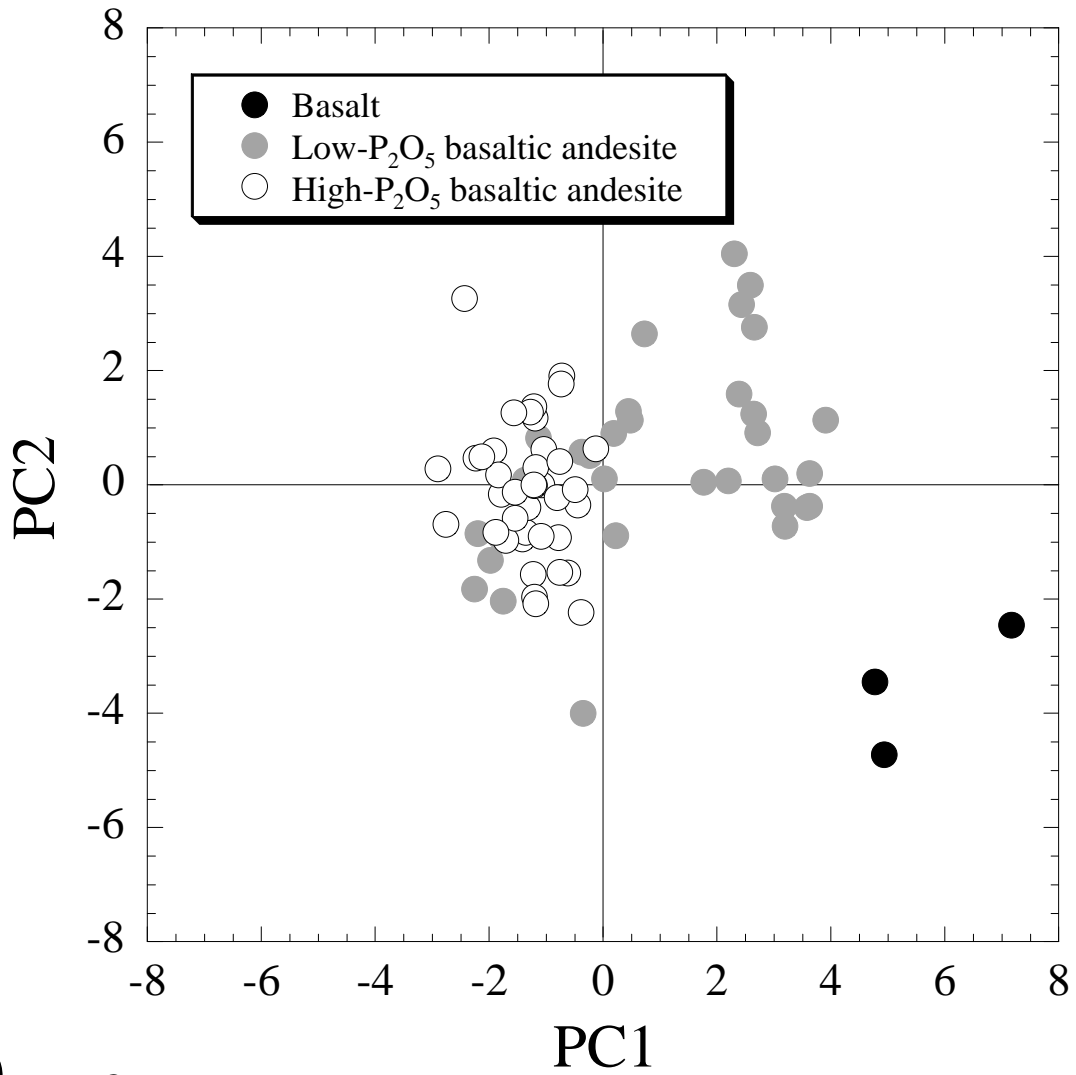


Figure 11

(a)



(b)

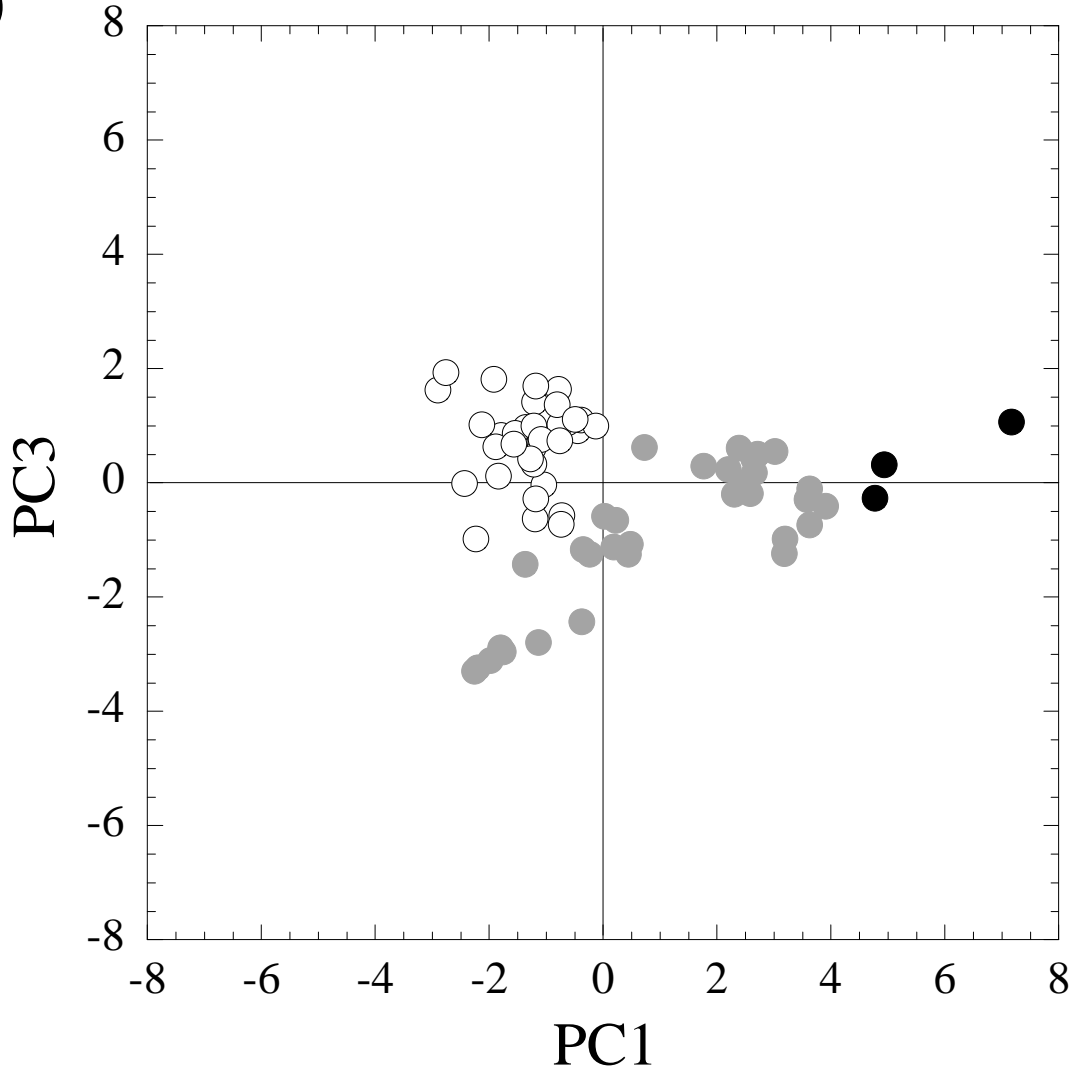


Figure 12

